HHS Public Access

Author manuscript

*Curr Biol*. Author manuscript; available in PMC 2025 July 22.

Published in final edited form as:

*Curr Biol*. 2024 July 22; 34(14): 3086–3101.e4. doi:10.1016/j.cub.2024.05.069.

# Dopamine neurons drive spatiotemporally heterogeneous striatal dopamine signals during learning

**Liv Engel**[1,2,3,*], **Amy R. Wolff**[1,2,*], **Madelyn Blake**[1], **Val L. Collins**[1,2], **Sonal Sinha**[4], **Benjamin T. Saunders**[1,2,5,6]

[1]Department of Neuroscience, University of Minnesota, 2001 6th St SE, Minneapolis, MN 55455, USA

[2]Medical Discovery Team on Addiction, University of Minnesota, 2001 6th St SE, Minneapolis, MN 55455, USA

[3]Current address: Department of Psychology, University of Toronto - Scarborough, 1265 Military Trail, Toronto, ON M1C 1A4, Canada

[4]Krieger School of Arts & Sciences, Johns Hopkins University, 3400 N. Charles St, Baltimore, MD 21218, USA

[5]X (formerly Twitter): @bensaunders

[6]Correspondence: bts@umn.edu

## Abstract

Environmental cues, through Pavlovian learning, become conditioned stimuli that invigorate and guide animals toward rewards. Dopamine neurons in the ventral tegmental area (VTA) and substantia nigra (SNC) are crucial for this process, via engagement of a reciprocally connected network with their striatal targets. Critically, it remains unknown how dopamine neuron activity itself engages dopamine signals throughout the striatum, across learning. Here, we investigated how optogenetic Pavlovian cue conditioning of VTA or SNC dopamine neurons directs cue-evoked behavior and shapes subregion-specific striatal dopamine dynamics. We used a fluorescent biosensor to monitor dopamine in the nucleus accumbens (NAc) core and shell, dorsomedial striatum (DMS), and dorsolateral striatum (DLS). We demonstrate spatially heterogeneous, learning-dependent dopamine changes across striatal regions. While VTA stimulation evoked robust dopamine release in NAc core, shell, and DMS, predictive cues preferentially recruited

**Lead Contact**: Benjamin T. Saunders, Assistant Professor, University of Minnesota, 2001 6th St SE, Minneapolis MN, 55455 bts@umn.edu.

*Denotes equal contribution

Author Contributions

Conceptualization: LE, ARW, and BTS. Investigation: LE, ARW, MB, and VLC. Formal Analysis: LE, ARW, SS, and BTS. Writing – Original Draft: LE, ARW, and BTS. Writing – Review & Editing: LE, ARW, and BTS. Visualization: LE, ARW, and BTS. Supervision: BTS. Funding Acquisition: VLC and BTS.



Declaration of Interests

The authors declare no competing interests.

dopamine release in NAc core, starting early in training, and DMS, late in training. Negative prediction error signals, reflecting a violation in the expectation of dopamine neuron activation, only emerged in the NAc core and DMS. Despite development of vigorous movement late in training, conditioned dopamine signals did not emerge in the DLS, even during Pavlovian conditioning with SNC dopamine neuron activation, which elicited robust DLS dopamine release. Together, our studies show broad dissociation in the fundamental prediction and reward-related information generated by VTA and SNC dopamine neuron populations and signaled by dopamine across the striatum. Further, they offer new insight into how larger-scale adaptations across the striatal network emerges during learning to coordinate behavior.

## eTOC Blurb

Engel, Wolff et al. examine how dopamine (DA) neuron mediated Pavlovian learning engages DA signals across the striatum. They find a spatiotemporally heterogenous landscape of DA encoding that is qualitatively distinct for VTA versus SNc DA neurons. These results offer broad insight into the functional architecture of the striatal network.

## Introduction

Animals are heavily influenced by external sensory information (“cues”) that acquires motivational value to trigger and guide complex behaviors. Midbrain dopamine neurons are crucial for learning and evaluation of cues, actions, and outcomes during decision making[1–5]. Dopamine neuron activity is evoked by rewards and can drive cue-based learning and motivation, with heterogeneous functions ascribed to different subcircuits[6–13]. Dopamine neurons project largely along an ipsilateral, ventromedial to dorsolateral gradient, with ventral tegmental area (VTA) neurons preferentially innervating the ventral and medial striatum, and substantia nigra (SNC) neurons preferentially innervating the dorsal and lateral striatum[14–16]. Through direct and indirect circuits back from the striatum to the midbrain, this network is thought to be functionally organized as an ascending “spiral”[16,17], where the locus of control of learning and behavioral execution transitions from dopamine inputs into the nucleus accumbens (NAc) to dopamine inputs into the dorsolateral striatum (DLS)[18–20]. This shift coincides with emergence of stereotyped, habitual action patterns after extended training[21–23]. Recent work has complicated this influential framework, however, with studies showing a lack of DLS recruitment[24,25], no reduction in NAc dopamine signaling[26,27], and a maintenance of NAc control of behavior late in conditioning[28]. There is also growing consensus of highly specialized dopamine signaling patterns and functional roles among dopamine projections and the striatal niches they innervate[6,8,26,29–40].

Despite the implications for a more complete understanding of the functional architecture of the striatal network, it remains unknown how dopamine neuron activity itself engages dopamine signals broadly throughout the striatum, across different learning phases. To investigate, we combined optogenetic manipulation of VTA or SNC dopamine neurons with simultaneous recording of dopamine transmission in different striatal subregions, using the biosensor dLight[41] and detailed behavioral analyses[42]. Dopamine neuron activation drove learning about antecedent cues, which came to evoke conditioned approach and rapid movement invigoration, similar to learning driven by external rewards[6,43,44]. Critically,

striatal dopamine dynamics were spatiotemporally heterogeneous and distinct for VTA versus SNC conditioning. Our results indicate that Pavlovian learning mediated by dopamine neuron activity leads to a preferential recruitment of cue-, reward, movement, and error-related dopamine signals in only a subset of striatal targets. Further, our data suggest that extended Pavlovian learning does not produce ventral-to-dorsal or dorsal-to-ventral shifts in dopamine signaling. Instead, different populations of dopamine neurons engage qualitatively distinct recruitment of striatal dopamine signaling during learning, across different timescales and with unique subregion-based profiles.

## Results

### VTA dopamine neurons drive cue learning and vigorous behavior

For dopamine neuron manipulation, we expressed the excitatory opsin Chrimson in TH-cre rats[6,45], and implanted optic fibers over the VTA (Figure 1A,B; Figure S1). To investigate the ability of sensory cues paired with dopamine neuron activation to drive behavior, we used an optogenetic Pavlovian conditioning procedure[6]. Rats were habituated to a neutral cue (light+tone, 7 sec), followed by 20 daily sessions where the cue was paired with VTA stimulation (589 nm, 20Hz, 2mW pulses, 5 sec) 25 times per session (Figure 1C). Laser stimulation began 2 sec after cue onset. No other reward or external stimuli were administered.

We first analyzed a subset of videos from training sessions (n=10 rats) via experimenter inspection. Rats quickly exhibited conditioned behavior (CRs), defined simply as locomotion, which increased in probability in the first 2-sec of cue presentations across training (Figure 1D; main effect of session, $F_{(1.53,13.04)}$=15.75, p=.0006). Onset latency of conditioned movement decreased with training, and the majority of CRs began before laser onset (Figure 1E; $F_{(1.84,11.93)}$=12.62, p=.0013). This is consistent with previous findings[6], indicating that CRs elicited by paired cues reflect learned behavioral responses, and not simply triggered by laser activation. We have previously demonstrated[6] that unpaired dopamine neuron activation in either the VTA or SNC is insufficient to drive cue learning, and does not evoke movement/other behaviors[27,46]. For detailed quantification of cue-evoked behavior across the whole dataset (n=20), we employed DeepLabCut[42] for movement analysis (Figure S1C–H). This revealed decreased latency to move (main effect of training phase, $F_{(1.7,28.8)}$=3.79, p=.041) and increased movement duration ($F_{(1.51,25.59)}$=22.04, p<.0001) across early (days 1–2), middle (days 10–12), and late (days 19–20) training. The average (Figure 1F,G) and maximum speed (Figure 1H) of conditioned movement increased across training ($F_{(1.81,30.81)}$=25.65, p<.0001; $F_{(1.928,32.78)}$=21.52, p<.0001). Further, the vigor of conditioned movement increased, reflected in decreased latency to achieve maximum speed (Figure 1I; $F_{(1.44,24.43)}$=327.9, p<.0001). These changes reflected a conditioned, cue-dependent invigoration, as speed during the 5 seconds before cue onset showed no changes across training (Average speed, $F_{(1.99,33.9)}$=.036, p=.964); Max speed, $F_{(1.92, 32.6)}$=1.44, p=.858). We analyzed behavioral data split by training phase and sex (12F, 8M; Figure S1I–O). The only sex difference was greater average speed in female rats, in both cue ($F_{(1,18)}$=4.42, p=.0499) and pre-cue ($F_{(1,18)}$=4.65, p=.045) epochs, throughout training.

The cue light allowed for localized, cue-directed CRs to occur in the form of orientation, approach, and investigation (Figure 1J), common behavioral responses to reward-predictive cues[47]. Experimenters recorded approach, which was evident early in training on ~30% of cue presentations and trended downward throughout conditioning (number: $F_{(2.79,23.73)}$=2.98, p = 0.0525; probability: $F_{(2.65,22.55)}$=2.87, p = 0.064). We further analyzed movement with DeepLabCut, and consistent with manual scoring, approach developed early in training and then downward throughout (Figure 1K, $F_{(1.716,29.17)}$=3.43, p = 0.052). On approach trials, rats spent less time engaged in cue approach (Figure 1L, $F_{(1.44,24.41)}$=11.07, p=.001) and the time spent interacting with the cue across all trials decreased (Figure 2M, $F_{(1.85,29.51)}$=5.00, p=.01).

We also quantified head orientation as a measure of cue-directed attention that did not meet approach criteria (Figure S1). The likelihood of cue orientation increased from early to later stages of training (% trials: $F_{(1.476,25.08)}$=9.05 p<.0.01), with a consistent latency ($F_{(1.71,29.14)}$=1.36, p=.27). However, on trials where rats oriented, the total time orienting (Figure 1N, $F_{(1.98,33.64)}$=8.88, p=.0008) and the duration of orientation (Figure 1O, $F_{(1.56,26.45)}$=5.53, p=.01) decreased significantly in the later stages of training. Thus, rats maintained attention to the cue but spent less time engaged in cue investigation.

As training progressed, we observed an evolution in conditioned behavior, where rats transitioned from predominantly linear movement often cue-directed, to more vigorous rotational behavior (Figure 1P, Figure S1). Rotations were cue-evoked, and always occurred contralateral to the stimulation site. Rotations never occurred in the first few sessions, indicating a learned conditioned response rather than an automatic laser-evoked movement pattern. Across middle/later training stages, cue-initiated rotations strongly emerged, increasing in number (Figure 1Q, $F_{(1.44,12.25)}$=12.83, p=.0019) and probability (Figure 1R, $F_{(1.98,16.84)}$=77.39, p<.0001). Using DeepLabCut, we interpolated angular speed, which increased across training (Figure 1S,T, average: $F_{(1.49,25.32)}$=30.38, p<.0001; maximum: $F_{(1.52,25.83)}$=6.68, p=.008).

## VTA dopamine mediated learning drives cue-evoked dopamine signals first in the core, then DMS, but not in shell or DLS

We used fiber photometry recordings of the dLight1.3b sensor[41] to measure dopamine signaling across four striatal regions: the NAc medial shell, NAc core, DMS, and DLS (Figure 2A,B). Across all sites, we found robust spontaneous dopamine signals (Figure 2C). To validate our approach, we compared the 465 and 405-nm signal channels across regions, showing robust signal-to-noise fidelity (Figure S2). Further, patterns were qualitatively similar when 465 signals were processed independent of 405-channel fitting, indicating that isosbestic fitting for delta F/F calculations did not artificially create region-specific activity patterns[48,49].

Spatially and temporally heterogeneous signals emerged in response to VTA dopamine neuron predictive cues (Figure 2D–H). Cue-evoked dopamine increases developed in the NAc core and the DMS, but not the medial shell or DLS. NAc core signals emerged first, early in training, and remained stable (Figure 2F & S3), whereas DMS signals emerged once behavior had largely stabilized (Figure 2G & S3). These signals both peaked ~800ms after

cue onset, before laser stimulation began. Despite the development of rapid and vigorously expressed cue-evoked movement, cue-conditioned dopamine signals in the DLS did not emerge (Figure 2H). Several peak signal metrics during the first 2-sec of cue presentations differed across regions and training phases, including peak Z-score (Figure 2I, interaction, $F_{(6,38)}$=3.14, p=.013; main effect region $F_{(3,21)}$=4.43, p=.015), area under the curve (AUC, Figure 2J, interaction, $F_{(6,38)}$=2.56, p=.035; region, $F_{(3,21)}$=5.26, p=.0073), and the rise (Figure 2K, interaction, $F_{(6,38)}$=4.11, p=.0033; region, $F_{(3,21)}$=4.60, p=.013) and fall slopes (Figure 2L, interaction, $F_{(6,37)}$=4.00, p=.0035; region, $F_{(3,21)}$=3.99, p=.022).

NAc shell and DLS cue-related signal AUCs remained near zero across training (Figure 2M, paired t-test for shell, $t_{(3)}$=1.0, p=.39; DLS, $t_{(8)}$=.47, p=.65). In the core, the peak Z-score (Figure 2N, $t_{(5)}$=.09, p=.48) did not change, but AUC increased (Figure 2M; $t_{(5)}$=2.05, p=.048) and fall slope decreased (Figure 2P, $t_{(5)}$=2.23, p=.038), suggesting prolonged cue-evoked dopamine release, or altered dopamine reuptake rate. In the DMS, the AUC (Figure 2M, $t_{(5)}$=2.55, p=.026) and peak Z-score (Figure 2N, $t_{(5)}$=2.18, p=.04) increased between early and middle/late training phases. The rise (Figure 2O, $t_{(5)}$=2.34, p=.033) and fall (Figure 2P, $t_{(5)}$=2.04, p=.048) slopes of the DMS signal also increased, suggesting increased rates of dopamine release and clearance.

We next examined relationships between cue-evoked dopamine and anatomical placement of recordings sites in the striatum, independent of regional subgrouping (Figure S4A). In the ventral striatum, cue-evoked signals were smallest medially and became larger moving toward lateral sites. A significant placement versus peak signal relationship was apparent early ($R^2$=.545, p=.015), and became stronger in late training ($R^2$=.613, p=.0074). The dorsal striatum, in contrast, showed no relationship between dopamine signals and anatomical placement ($R^2$=.104, p=.24) initially. However, a significant relationship developed late in training ($R^2$=.446, p=.0065), where larger cue-evoked signals were measured medially and became smaller as placements moved laterally. Within-subjects, spontaneous cue responses in early training were not significantly correlated with responses later in training (p=.943), indicating that they emerge as a function of learning.

Additional analysis focused on the relationship between cue signals in the core and DMS and the emergence of conditioned behavior (Figure 3). We pooled trials in the early versus mid/late training phases across rats and plotted the peak cue-evoked signals with trials sorted by average speed. These show that cue-evoked signals in the core were evident early in training but did not vary with speed (Figure 3A, faster trials on top). In later training, stronger, more enduring signals emerged following cue onset on faster movement trials (Figure 3B). Accordingly, NAc core cue-evoked signals were not correlated with movement vigor early in training (Figure 3E; max speed p=.901, avg speed p=.955, latency to max p=.739), but became consistently correlated at the mid (Figure 3F; max p=.001, avg p=.0002, latency to max p=.817) and late (Figure 3G; max p=.013, avg p=.0027, latency to max p=.039) training phases Not surprisingly, DMS responses were not correlated with movement across training (Figure 3H–J), except a positive correlation with max speed in late training (Figure 3J, p=.0013). Collectively, this suggests dopamine signals evoked by the predictive cue in the NAc core encode features of conditioned movement vigor earlier, and preferentially, compared to DMS signals.

## VTA dopamine neuron activation evokes DA signaling preferentially in medial striatum

We next explored how VTA dopamine neuron activity alters dopamine signaling across the striatum (Figure 4). During photometry sessions, cues were paired with laser stimulation on 80% of trials. Focusing on the stimulation window, we quantified the average Z-score and AUC, which varied by region and training phase (Figure 4F,G, interaction, $F_{(6,38)}$=17.9, p<.0001); main effect of region, $F_{(3,21)}$=9.11, p=.0005). In the medial shell, dopamine signals were largest, and increased across training (Figure 4B,F,G; Figure 4H, $t_{(3)}$=3.01, p=.029), which did not occur elsewhere. In the core (Figure 4C,F,G; Figure 3H, $t_{(5)}$=.939, p=.196) and DMS (Figure 4D,F,G; Figure 4H, $t_{(5)}$=.762, p=.24), laser-evoked dopamine signals were stable. In the DLS, we saw little laser-evoked dopamine, which decreased with training (Figure 4E,F,G; Figure 4H, $t_{(8)}$=2.35, p=.047). Given the uniquely large signal in the shell, we separately analyzed signals with the shell excluded and differences across region and training phase were maintained (Interaction, $F_{(4,33)}$=4.15, p=.0078; main effect of region, $F_{(2,18)}$=11.53, p=.0006).

We next examined the relationship between VTA dopamine neuron stimulation and evoked dopamine signals across the striatal space, independent of subgrouping (Figure S4B). We found an overall gradient of laser-evoked dopamine in the coronal plane, with signal magnitude shrinking along the ventromedial (largest) to dorsolateral (smallest) axis. Early in training, there was a trend for a correlation between recording placement and dopamine signal ($R^2$=.14, p=.064), which became highly significant by late training ($R^2$=.41, p=.0005). Within-subjects, stimulation-evoked dLight early in training was highly correlated with the signal evoked by laser later in training (p=.0003), indicating stability of activation throughout the experiment. We found no relationship between variability in stimulation fiber placements, which were clustered over central VTA (mean fiber location +0.69mm lateral; Figure 1B), and dopamine stimulation magnitude (Early: p=.411; Late: p=.216).

## Dopamine signals in the NAc core and DMS, but not shell or DLS, report dopamine prediction errors

We next assessed whether striatal dopamine signals report a violation in the expectation of dopamine neuron activation (Figure 5). On 20% of trials during photometry sessions cues were presented but laser stimulation was omitted (Figure 5A). Rats behaved similarly on omission and stimulation trials, moving in response to cues for the same percentage of time (Figure 5B, $F_{(1,19)}$=1.81, p=.195), and reaching the same maximum speed across training ($F_{(1,19)}$=.748, p=.398). This further underscores that behavior reflected learned conditioned responses rather than simple laser-evoked movements. On omission trials, movement was tightly locked to cue-presentations (Figure 5C) and increased across training (Figure 5D–F; avg speed, $F_{(1.70,27.11)}$=23.8, p<.0001; max speed, $F_{(1.54,24.61)}$=19.04, p<.0001; time to max, $F_{(1.48,23.72)}$=61.6, p<.0001), similar to stimulation trials (Figure 1).

Dopamine signals during omission windows varied by region and training phase (Figure 5K, avg Z score, interaction, $F_{(3,21)}$=3.129, p=0.04; Figure 5L, AUC, trend for interaction, $F_{(3,21)}$=2.76, p=.068, main effect of region, $F_{(3,21)}$=3.34, p=.039). During the window of omission of expected dopamine neuron excitation, dopamine signals in the NAc core and DMS dipped below baseline (Figure 5H,I), consistent with a negative prediction error. These

error signals were not present at the beginning of training, but developed in later phases (Figure 5M, core, $t_{(5)}$=4.03, p=.005; DMS, $t_{(5)}$=2.31, p=.035), echoing dopamine response patterns when natural rewards are omitted[50–52]. In contrast, dopamine signals in the shell and DLS were unresponsive to laser omission (Figure 5G,J,M). Taking our cue-response data (Figure 2) and omission data (Figure 5) together, we find that only the NAc core and DMS engage in prediction error-like dopamine signaling based on learning driven by VTA dopamine neuron activity.

## Pavlovian learning driven by SNC dopamine neuron stimulation directs unique, heterogeneous striatal dopamine signals

Our results show that learning driven by VTA dopamine neurons does not recruit DLS dopamine signals. Critically, stimulation of SNC dopamine neurons is also sufficient to drive Pavlovian learning, but the content and behavioral impact of that learning is distinct from that engaged by VTA dopamine neurons[6,10,53]. To build on this notion, we explored the striatal dopamine impact of optogenetic conditioning of SNC dopamine neurons. In a new cohort, stimulation was targeted to SNC dopamine neurons (Figure S1, mean fiber location +2.2mm lateral) and conditioning was completed as above (Figure S5). Similar to VTA conditioning, we found cues predicting SNC dopamine neuron activation drove robust learning, as quantified by increased likelihood of movement and speed during cue presentations (Figure S5D). The average and maximum speed of cue-conditioned movement increased across training (Figure S5E,F; $t_{(9)}$=3.75, p=.005, $t_{(9)}$=3.21, p=.011). As training progressed, we saw reduced cue-directed approach (Figure S5G, $F_{(1.88,11.25)}$=4.15, p = 0.046), and increased rotations (Figure S5H,I, $F_{(1.46,11.42)}$=11.42, p = 0.0046). As with VTA rats, SNC conditioned turning behavior was cue-evoked and contralateral to the stimulation site.

During this SNC dopamine optogenetic conditioning (Figure 6A), we recorded dLight dopamine signals in the striatum. We focused on the NAc core (n=9) and the DLS (n=5), as these regions showed the most distinct patterns with VTA conditioning, and it remains unknown whether SNC dopamine neurons engage dopamine signaling in the ventral striatum during learning. Spatially and temporally heterogeneous dopamine signals emerged in response to SNC dopamine neuron predictive cues (Figure 6B–I). Brief cue-evoked dopamine increases occurring in the NAc core early in training diminished as conditioning progressed (Figure 6B). In the DLS, no cue-evoked response was seen initially, but a slow negative ramp following cue onset emerged later (Figure 6C). We quantified cue-evoked signals, which varied systematically in peak and AUC (Figure 6D,G,E,I; peak: interaction, $F_{(2,12)}$=5.44, p=.038; AUC: trend main effect of phase, $F_{(1,12)}$=4.44, p=.056). Peak signals in the NAc core diminished, while the DLS peak remained near zero (Figure 6G, core, $t_{(8)}$=2.55, p=.034; DLS, $t_{(4)}$=1.72, p=.16). The AUC of cue-evoked dopamine signals was slightly negative in the core, and remained stable (Figure 6H, $t_{(8)}$=.329 p=.75). In contrast, DLS dopamine became more negative with training (Figure 6H, AUC, $t_{(4)}$=5.04, p=.007; trough/minimum, $t_{(4)}$=6.22, p=.003). We examined the relationship between SNC cue-related signals and behavior on a trial-by-trial basis (Figure S5). While initial NAc cue peak signals were positively correlated with movement speed (p=.0001), this relationship

went away as training progressed. Cue-evoked negative ramps in DLS dopamine were not correlated with movement variables at any stage.

During the stimulation window, optogenetic activation of SNC dopamine neurons produced variable dopamine responses across recording sites (Figure 6B,C,F,I; $F_{(1,12)}$=140.4, p<.0001). In the core, dLight signal remained near zero during simulation (Figure 6F,I; $t_{(8)}$=.162, p=.86). In the DLS, strong laser-evoked dopamine signals were consistent across phase (Figure 5F,I; $t_{(4)}$=.89, p=.42). For further comparison of learning-related dopamine signals in the NAc core and DLS, we plotted data for VTA and SNC conditioning together (Figure S6). This showed that learning driven by VTA versus SNC dopamine neurons, despite promoting strong conditioned behavioral invigoration in either case, results in nearly diametrically opposed dopamine signals in the dorsal and ventral striatum.

We next examined dopamine signals during SNC laser omission trials (Figure 6J,K,L), finding different patterns in the core and DLS across phases (Figure 6M–P; avg Z-score interaction, $F_{(1,20)}$=4.80, p=.039; main effect of region, $F_{(1,20)}$=6.49, p=.019; AUC interaction, $F_{(1,20)}$=4.84, p=.04). In the NAc core, omission of SNC dopamine neuron stimulation had no effect on dopamine signals, which remained at zero/baseline (Figure 6O,P; avg Z-score, $t_{(8)}$=.209, p=.84; AUC, $t_{(8)}$=.28, p=.79). In contrast, negative DLS dopamine signals during the omission window emerged across training (Figure 6O,P; avg Z-score, $t_{(4)}$=3.38, p=.028; AUC, $t_{(4)}$=3.39, p=.0275). Based on qualitative inspection of the DLS omission traces (Figure 6L), increasingly negative Z-score and AUC values during the omission window appear to reflect that the DLS signal was already negative following cue onset, an effect that grew across conditioning. This suggests that omission related DLS signals following SNC conditioning are potentially unique from those seen in the core and DMS during VTA conditioning (Figure 5), and do not necessarily indicate a negative prediction error.

## Discussion

Here, we investigated the impact of learning engaged by dopamine neurons. Recording dopamine signals across striatal regions during optogenetic Pavlovian conditioning, we show there is considerable heterogeneity in the extent that VTA and SNC dopamine neurons drive learning-related dopamine signals downstream. By targeting dopamine neurons directly, our results offer insight into their fundamental contributions in this domain - independent of the slew of brain and body processes that are recruited during conditioning with naturally consumed rewards, like food. Below, we discuss how these results shape our understanding of striatal dopamine function and the *in vivo* circuit architecture of the midbrain-striatum network.

### Specialized cue, error, and reward signals across striatal dopamine targets

Dopamine signals in response to cues predicting VTA dopamine neuron activation developed in the NAc core and DMS on different timescales. Core signals were uniquely apparent at the beginning of conditioning when cue-evoked movement patterns were less vigorous and more cue-directed. Our data suggest the function of the NAc core signal evolves over time, where early signals reflect some aspect of novelty or general salience[54]

and later signals reflect motivational vigor. We also found error-related signaling in these regions, where dopamine signals dipped below baseline precisely when dopamine stimulation was omitted, only after learning had occurred. The fact that this type of striatal plasticity can be engaged in the absence of learning driven by interface with a natural reward suggests that it is a fundamental feature of the system. The lack of error-related DLS dopamine fits with evidence that dopamine neuron axons in the DLS are less responsive to negative prediction errors compared to other regions[30].

We conclude that NAc core and DMS dopamine are unique among striatal subregions in prioritizing encoding of expectation-related information, consistent with aspects of previous studies using natural reward conditioning[30,31,39,40]. The broad similarity we see in NAc core and DMS dopamine signals during Pavlovian learning is interesting in light of studies that show DMS and core dopamine signals diverge and have unique functional roles during instrumental decision making tasks[29,55,56]. One possibility is that while nominally similar to the core, the DMS cue signals in our studies could be more related to action values and action prediction, which reflect learned cues and decision states that function somewhat independent of reward value or reinforcement[55,57–59]. The fact that we saw tighter relationships between cue-evoked dopamine and behavioral invigoration in the core versus the DMS supports a framework where core signals preferentially encode motivational features of Pavlovian cues[44,60,61]. Major differences for the role of VTA and SNC dopamine neurons in reinforcement, cue valuation, and model-based learning are becoming clear[6,7,10,53], but more direct comparisons between DMS and NAc core projecting dopamine neurons are needed.

Previous studies using functional imaging to measure brain-wide activation generated by dopamine neuron indicate that dopamine neurons can alter network level activity[62,63]. Notably, we found robust VTA laser-evoked dopamine signals in the DMS (but not DLS), in addition to the NAc core and shell. This suggests dopamine neurons projecting to the NAc and DMS are somewhat intermingled in the VTA/medial SNC, allowing for an interface between dopamine circuits innervating in the medial portion of the striatum across the dorsal-ventral axis. This is also supported by anatomical work[14,15], but it will be important to compare our results with future studies targeting VTA dopamine neurons that project only to the NAc.

In the NAc medial shell, we found a unique dopamine pattern. There was no evidence of either cue or error-related signals, but instead, the largest laser-evoked dopamine signals. This motivates an important conclusion borne out by several features of our data: the degree to which a striatal site can be conditioned to encode cue-related information is not simply a reflection of how much dopamine is stimulated there. Notably, our data reflect dopamine recordings in only the dorsal portion of medial shell, and conditioned stimuli evoke unique encoding mechanisms along a dorsoventral axis within the medial shell[33,64,65]. Recent evidence indicates anatomically localized functions for the shell may be due to unique terminal mechanisms[66], as well as specific patterns of midbrain connectivity[33,67,68], compared to other parts of the ventral striatum. Overall our results fit with the notion that dopamine in the ventromedial striatum preferentially signals reward over other features of

learning[39,69–72]. They also support anatomical frameworks classifying the medial shell as part of a distinct brain macrosystem within limbic networks[73,74].

The results from our SNC conditioning experiments motivate some important considerations. First, we find that optogenetic stimulation of SNC dopamine neurons does not evoke dopamine release in the NAc core, and SNC-predictive cues do not drive conditioned dopamine responses or prediction errors in the core. These results give an *in vivo* explanation for why, across a slew of studies, and in classic frameworks of dopamine heterogeneity, SNC dopamine manipulations are shown to support fundamentally different learning processes[2,4,6,10,53,57,60,75]. SNC dopamine neurons are generally unable to imbue cues and actions with conditioned value to promote flexible reward seeking, a function that seems to rely on or require activity in VTA dopamine neurons projecting to the ventral striatum. The presence of novelty-related cue responses in the core early in SNC dopamine conditioning, which diminished as training progressed, lends further support to the notion that early responses in the core are qualitatively different from those emerging later in training in the VTA conditioning groups. Critically, we show that at least some forms of Pavlovian learning do not require the development and maintenance of cue-evoked dopamine signatures in the NAc core.

We find unique cue evoked DLS signals in response to learning driven by SNC dopamine neurons. Despite strong laser-evoked dopamine release and robust conditioned behavior, dopamine responses to the SNC-predictive cue became negative across training. Based on the current results alone, these conditioned negative ramps are difficult to fully explain. Phasic activation of SNC dopamine neurons is strongly reinforcing[6,10,53,76], and fluctuations in DLS dopamine are thought to facilitate exploration and movement sequences[8,77,78], so it is unlikely that negative cue signals here reflect negative valence. Instead, this DLS dopamine signature may stem from the unique striatal network engagement that SNC dopamine neurons promote, compared to VTA dopamine neurons, including terminal mechanisms that briefly suppress DLS dopamine signaling during learning. SNC cell body recording studies have shown mixed results, with examples of both increases and decreases in dopamine cell firing before movement initiation[27,79,80], and subtypes of SNC dopamine neurons respond to movement and reward differently[38]. In other studies, fluctuations in cholinergic interneurons gate dopamine release in the dorsal striatum via glutamatergic inputs[81–83]. Future studies will be needed to parse these factors, but regardless of the specific mechanism, our results support a framework where VTA and SNC dopamine neurons orchestrate qualitatively different learning processes, via unique recruitment of striatal dopamine.

## Implications for understanding the functional architecture of the midbrain-striatum network

By isolating the impact of learning driven directly by dopamine neurons, our results offer insight on long-standing questions about the functional organization of the striatal network, vis-a-vis the “ascending” spiral framework[16,17], where neural signals transition from VTA inputs to the ventral striatum to SNC inputs to the dorsal striatum[18–20] in parallel with extended learning[21]. We show that rather than a shift *away* from ventral striatum, an

additive, progressive recruitment of DMS occurs instead[31]. This recruitment was limited to medial dorsal regions and did not encompass the DLS. Overall, our work is more consistent with recent *ex vivo* studies demonstrating that DMS-projecting dopamine neurons do not have circuit-level functional connectivity with DLS-projecting dopamine neurons[84]. Rather, midbrain-striatal systems exist as reciprocal, parallel, primarily independent loops, where VTA dopamine neurons can control their own (but not SNC) activity via direct pathway projections from the ventral striatum[17,67,84–86]. An implication of this past work is that there is no pre-existing connectivity to support an ascending DLS engagement, but that learning drives plasticity that recruits a spiral mechanism. Our work explores this notion *in vivo*, and we find little direct evidence: despite extended VTA neuron driven Pavlovian learning that produces rapid cue-evoked movement patterns, neither cue nor robust laser-evoked dopamine signals emerge in the DLS. Further, NAc core dopamine signals became more correlated with conditioned movement across training. Consistent with this, in previous studies NAc, but not DLS dopamine remains robust and important for execution of conditioned cue approach after learning[28,31]. This is not restricted to Pavlovian learning, as other recent work highlights a lack of shift toward DLS dopamine signals and striatal activity during the development of outcome-insensitive instrumental habits[24–26]. Our SNC conditioning experiments further indicate that “descending” recruitment of ventral striatum is not engaged by learning driven by dorsal striatum dopamine inputs[84]. Collectively, our data support an updated account of the functional architecture of midbrain-striatal loops, where learning is not predicated on a consistent shift along the ventromedial to dorsolateral axis, or vice versa, in dopamine signaling.

It is important to consider our results in the context of seminal studies demonstrating a clear shift in striatal recruitment to the DLS[19,20,87,88]. The strongest evidence comes from instrumental conditioning where cocaine is self-administered for extended periods, suggesting that chronic dopamine system hyperactivation via drug stimuli may be necessary to promote DLS recruitment. Actual commerce with external reward is perhaps not essential, however, as extended dopamine neuron self-stimulation can promote plasticity in the dorsal striatum that is similar to that produced by cocaine self-administration[89,90]. Thus, DLS recruitment may depend on whether mesolimbic dopamine circuits are activated in a rapid, binge-like, or escalating fashion. Another possibility is that DLS is recruited independent of dopamine signals, including through potentiation of corticostriatal inputs[91,92]. Recent efforts have also characterized functionally distinct roles for striatal output pathways in behavioral control, via parallel channels through the thalamus, midbrain, and cortex[86,93,94]. It will be important to investigate how dopamine neuron activity may engage such broader nigro-thalamo-cortical and striatal loops, which could provide a circuit mechanism by which midbrain inputs to the ventral striatum can engage dorsal striatum, beyond the classic spiral mechanisms. The recent discovery of pan-striatal wave-like activation patterns among dopamine terminals and cholinergic interneurons provides another possible source of ventral-dorsal interactions[95,96].

Here, we uncover fundamental region-specific patterns of dopamine signaling engaged during Pavlovian learning by measuring dopamine signals and behavior emergent from learning driven by different dopamine neuron populations, in the absence of other rewards. As learning progresses, a broader landscaping of dopamine release patterns emerges across

the striatum to uniquely signal movement, reward, and prediction-related features of learning. This work provides new insight into dopamine heterogeneity and the functional architecture of the striatal network, building on long-standing anatomical and *in vivo* recording frameworks.

## STAR★Methods

### Resource availability

**Lead contact—**Further information and requests for resources and reagents should be directed to and will be fulfilled by the lead contact, Dr. Benjamin Saunders (bts@umn.edu).

### Materials availability

This study did not generate new unique reagents.

### Data and code availability

- All data reported in this paper will be shared by the lead contact upon request.
- This paper does not report original code.
- Any additional information required to reanalyze the data reported in this paper is available from the lead contact upon request.

### Experimental model and study participant details

**Subjects—**Male and female TH-cre transgenic rats (n=30; 18F, 12M) bred on a Long-Evans background were used. These rats express Cre recombinase under the control of the tyrosine hydroxylase (TH) promoter[45]. All rats weighed 250–500g at the time of surgery and were 4–7 months old at the time of experimentation. Experimental procedures were approved by the Institutional Animal Care and Use Committee at the University of Minnesota and were carried out in accordance with the guidelines on animal care and use of the National Institutes of Health of the United States.

### Method Details

**Surgical Procedures—**Rats were anesthetized with 5% isoflurane and placed in a stereotaxic frame, after which anesthesia was maintained at 1–3%. Rats were administered saline, carprofen anesthetic (5 mg/kg), and cefazolin antibiotic (70 mg/kg) subcutaneously prior to start of surgery. The top of the skull was exposed and holes were made for viral infusion needles, optic fiber implants, and 4 skull screws. A total of 1.2 µL of virus (pAAV5-Syn-FLEX-Chrimson-tdTomato, Addgene) was infused unilaterally into the VTA (−5.6 AP, +/− 0.7 ML, −8.0 DV). In the same hemisphere, a virus coding for the dopamine biosensor dLight[41] (AAV5-hSyn-dLight1.3b, University of Minnesota Viral Vector and Cloning Core) was infused into the NAc (1.3 AP, +/− 1.3 ML, −7.0 DV), DMS (1.3 AP, +/− 1.3 ML, −4.3 DV), or DLS (1.7 AP, +/− 4.0 ML, −5.0 DV) at a total volume of 0.8 µL. A separate group of rats received the same Chrimson virus targeted to the SNC (−5.6 AP, +/− 2.5 ML, −7.5 DV) and dLight injections targeted to the ipsilateral DLS or NAc core. All viruses were infused at 0.1µL/min. Immediately after injection, the needle was raised 100 µm and then left in place for an additional 10 min to allow for diffusion. Optical fibers (9mm length, 400µm

diameter, Doric Lenses) for photometry recordings were chronically implanted into the NAc (1.3 AP, +/− 1.3 ML, −6.6 DV), DMS (1.3 AP , +/− 1.3 ML, −4.3 DV), or dorsal striatum (1.7 AP, +/− 4.0 ML, −4.4 DV), and optic fibers (10mm length, 300μm diameter, Thorlabs) for optogenetic stimulation were implanted above the VTA (−5.6 AP, +/− 0.7 ML, −7.9 DV) or SNC (−5.6 AP, +/− 2.5 ML, −7.3 DV) in the same hemisphere as the viral infusions. All coordinates are in mm relative to bregma and skull surface. Implants were secured to the skull with dental acrylic (Lang Dental) applied around the skull screws and the base of the ferrules containing the optic fibers. At the end of all surgeries, topical anesthetic and antibiotic ointment were applied to the surgical site, rats were placed on a heating pad and monitored until they were ambulatory. After surgery rats were individually housed with ad libitum access to food and water on a 0800 to 2000 light/dark cycle (lights on at 0800), given carprofen (5 mg/kg) and cefazolin (70 mg/kg) for the first 3 days following surgery and weighed and monitored for 6 days. Optogenetic manipulations commenced at least 4 weeks after surgery. Post hoc validation of optic fiber placements revealed subsets of rats with fibers targeted to the core versus medial shell of the NAc, which we analyzed separately.

**Optogenetic Stimulation—**Optogenetics studies used 589 nm lasers (OptoEngine and Dragon Lasers). Light output during individual 5-ms light pulses was adjusted to be approximately 2 $mW/mm^2$ at the tip of the intracranial fiber (10–20mW constant power). For all optogenetic studies, optic tethers connecting rats to the rotary joint were sheathed in a lightweight armored jacket to prevent cable breakage and block visible light transmission. Laser pulses were initiated from Med-PC TTL pulses and patterned via Synapse software that also controlled photometry and video data acquisition.

**Fiber Photometry—**To assess dopamine signaling across the striatum during Pavlovian conditioning, we measured dLight fluorescence in the NAc core, NAc shell, DMS, and DLS using fiber photometry. A fluorescence mini-cube (Doric-Lenses) transmitted light streams from 465 nm and 405 nm LEDs (Doric-Lenses), sinusoidally modulated at 211 Hz, and 330 Hz, respectively. LED power was set at ~100 μW. On recording days rats were tethered to a core, shell, DMS, or DLS implant using a low autofluorescence cable sheathed in a lightweight armored jacket (Doric-Lenses). On all photometry recording days the rats were simultaneously tethered to the VTA or SNC implant. Photometry recordings were conducted on specific days with interspersed recording free days. Recording data here are sampled from the early (day 1 and 2), middle (days 10 12) and late (day 19 and 20) stages of Pavlovian conditioning.

Fluorescence from below the fiber tip was transmitted back to the mini-cube, where it was passed through a GFP emission filter, amplified, and focused onto a high sensitivity photoreceiver (Newport, Model 2151). A real-time signal processor (RZ5P, Tucker Davis Technologies) running Synapse software modulated the output of each LED and recorded photometry signals, which were sampled from the photodetector at 6.1 kHz. Demodulation of the brightness produced by the 465-nm excitation, which stimulates dopamine-dependent dLight fluorescence, versus isosbestic 405-nm excitation, which stimulates dLight in a dopamine-independent manner, allowed for correction for bleaching and movement artifacts.

Task events (e.g., cue and laser presentations), were time stamped in the photometry data file via a TTL signal from the Med-PC behavioral program, and behavior was video recorded at 10–20 FPS, with timestamps for each frame captured in the photometry file.

**Habituation and Optogenetic Pavlovian Training—**Optogenetic Pavlovian training was conducted[6]. Briefly, rats were first acclimated to the behavioral chambers (Med Associates), conditioning cues, and optic cable tethering in a ~30-min habituation session. During this session, rats were tethered to a rotary joint and 20 cue presentations, with no other consequences, were presented on a 90-s average variable time (VT) schedule. In each of the subsequent conditioning sessions, rats were presented with 25 cue (light + tone, 7 s) – laser stimulation (100 5-ms pulses at 20 Hz; laser train initiated 2 s after cue onset and continued for duration of cue) pairings delivered on a 100-sec VT schedule. The sessions lasted ~42 min. These cues were never associated with another external stimulus (e.g., food or water). Cue and laser delivery were never contingent on an animal's behavior and all rats received the same number of cue and laser events. On photometry recording days, 20% (5/25, pseudorandomly delivered) of trials served as dopamine omission probes, wherein cues were presented as normal, but laser stimulation did not occur.

**Video Scoring—**During Pavlovian conditioning sessions behavior was video recorded using cameras (Vanxse CCTV Security Camera) positioned a standardized distance above each chamber. Videos from sessions 1, 2, 4, 8, 11, 12, and 19, 20 were scored offline by observers who were blind to the identity and anatomical target group of the rats. For days 1, 4, 8, 12, and 20, each cue-only (2-sec, 25 per session) and cue+laser (5-sec, 20 per session) event was scored for the occurrence and onset latency of the following behaviors. *Locomotion*: Defined as the rat moving all four feet in a forward direction (i.e., not simply lifting feet in place). *Cue Approach*: Defined as the rat's nose coming within 2.5 cm of the cue light. Approach often involved the rat moving from another area of the chamber to come in physical contact with the cue light while it was illuminated. *Rearing*: Defined as the rat lifting its head and front feet off the chamber floor, either onto the side of the chamber, or into the air. *Rotation*: Defined as the rat making a complete 360-degree turn in one direction. For cue approach and rotation, the number of occurrences were also scored. For days 2, 11, and 19, only locomotion was scored.

**Histology—**Rats were deeply anesthetized with sodium pentobarbital (2 mL/kg) and transcardially perfused with cold phosphate buffered saline followed by 4% paraformaldehyde. Brains were removed and post-fixed in 4% paraformaldehyde for ~24 hours, then cryoprotected in a 25% sucrose solution for at least 48 hours. Sections were cut at 50 microns on a cryostat (Leica CM1900). To confirm viral expression and optic fiber placements, brain sections containing the midbrain were mounted on microscope slides and coverslipped with Vectashield containing DAPI counterstain. Fluorescence from Chrimson and dLight as well as optic fiber damage location was then visualized using a Keyence BZ-X microscope.

## Quantification and statistical analysis

**DeepLabCut pose estimation—**Markerless tracking of animal body parts was conducted using version 2.2.1.1 of the DeepLabCut (DLC) Toolbox[42,97] and analysis of movement features based on these tracked coordinates was conducted in Matlab R2020b (Mathworks). All DLC analysis was conducted on a Dell G7–7590 laptop running Windows 10 with an Intel Core i7–9750H CPU, 2.60Ghz, 16 GB RAM, and an NVIDIA GeForce RTX 2080 Max-Q 8GB GPU. DeepLabCut 2.2.1.1 was installed in an Anaconda environment with Python 3.8.4, CUDA 11.7 and Tensorflow 2.10.

**DeepLabCut Model:** 2090 frames from 35 videos (32 different animals, 3 experiments) were labeled and 807 outlier frames were relabelled to refine the network. Labeled frames were split into a training set (95% of frames) and a test set (5% of frames). A ResNet-50 based neural network[98] was used for 1,030,000 training iterations. After the final refinement we found the test error was 4.1 pixels, the training error was 3.13 pixels and with a p-cutoff of 0.85 training error was 2.99 pixels and test error was 3.68 pixels. The body parts labeled included the nose, eyes, ears, center of head or fiber optic implant, shoulders, tail base, and an additional three points along the spine. Features of the environment were also labeled, including the 4 corners of the apparatus floor, two nose ports, two cue lights, two magazine ports, and 3 LED indicator lights when active (see Figure S1 for examples of labeled body parts and environment features).

**Behavior Analysis.:** DLC coordinates and confidence values for each bodypart and frame were imported to Matlab and filtered to exclude body parts/features from any frame where the confidence was < 0.7. For labeled features of the environment, which have a fixed location, the average coordinates for that recording were used for analysis. To convert pixel distances to the real chamber dimensions, for each video, a pixel to cm conversion rate was determined. The distance (in pixels) between each edge of the environment floor and the diagonal measurements from corner to corner were measured, and these values were divided by the actual distance in cm. The mean of these values was then used as the conversion factor. Movement speed was calculated from the implant coordinates frame by frame using the formula: [distance moved (pix per cm) * framerate] to give movement speed in cm/s. For plotting of speed data across recordings with different sampling rates, missing data points for the lower sampling rate sessions were filled in using linear interpolation with the interpol1 function (MATLAB), interpolated data points were not used to calculate peak or mean speeds for analysis. Approach to the cue light was detected by finding frames in which the nose was within 2.5 cm from the cue. The beginning and end of each approach occurred when the nose was further than 4.5 cm from the cue for 0.2s. Only approaches longer than 0.2 s were considered. Locomotion was detected using the speed of the 4 positions on the spine to detect whole-body movements. The movement threshold for detecting locomotion was calibrated to animal size using a scale factor determined from the relationship between body size (distance between the shoulder and mid-back points) and the optimal threshold for detecting movement in a separate group of animals not used for this study ($n = 4$). Locomotion bouts were detected when all visible body parts were above the movement threshold and a sliding window was used to determine when the speed of 2 or more body parts reached less than 50% of the detection threshold for 0.3s, indicating the beginning and

end of a movement. Movements less than 0.5s in duration were excluded. Orientation toward the cue light was determined by calculating the angle between the vector from the implant to the nose with the vector from the implant to the cue. Animals were labeled as oriented to the cue whenever this angle was <30° for more than 0.2s.

**Photometry data collection and analysis—**Photometry data was analyzed using a custom MATLAB pipeline, based on established methods for dLight data[24,41,54] and example code provided by TDT (Lick Bout Analysis.m). For analysis, signals were filtered with a 2-Hz lowpass filter, downsampled to 40 Hz, and a least-squares linear fit was applied to the 405-nm signal, to align it to the 465-nm signal. This fitted 405-nm signal was used to normalize the 465-nm signal, where ΔF/F = (465-nm signal – fitted 405-nm signal)/(fitted 405-nm signal). Normalized signals for each trial were extracted for 5s before and 10s after each cue presentation and Z-scored to the 5s pre-cue period for each trial to minimize the effects of drift in the signal across experiment duration. Cue responses were detected in the average trial waveform for each animal in the 2s window beginning at cue onset (and prior to optogenetic stimulation). Responses to the presence or absence of optogenetic stimulation were detected in the average trial waveforms for each animal across the 5s stimulation window, beginning 2s after cue onset. The maximum and minimum responses in each window were detected and latency was calculated relative to the start of the detection window. In some cases, the peak signal did not change, and so we also calculated waveform slopes, as a proxy for other features of dopamine signaling dynamics. The slope of the rising and falling phase of the peak and trough waveforms were calculated between the maximum and 50% of max using the formula t2−t1/f2−f1, where t is the beginning and end timepoints of the rising or falling phase of the waveform, and f is the Z-scored fluorescence at each timepoint. Area under the curve (AUC) values were calculated from the Z-scored traces by numerical integration via the trapezoidal method using the trapz function (Matlab). Peak and AUC of cue responses were calculated in the window after cue onset, before laser stimulation, to quantify the magnitude of cue-related signal changes. AUC for the stimulation window was calculated over the laser-on window. Recording groups were as follows: VTA-Dopamine conditioning: NAc shell (n=4), NAc core (n=6), DMS (n=6), and DLS (n=9); SNC-Dopamine conditioning: NAc core (n=9), DLS (n=5).

**Statistics—**Behavior and photometry signal data were analyzed with a combination of linear mixed-effects ANOVA models, planned t tests, and Pearson correlations. Post-hoc comparisons were completed with Bonferroni corrections. Summary graphs represent averages of recordings sites/subjects, not individual trials. The data are expressed as the mean ± s.e.m. Statistical significance was set at $p<0.05$.

## Supplementary Material

Refer to Web version on PubMed Central for supplementary material.

## Acknowledgments

This work was supported by NIH grants F32 DA051138 (VC) and R00 DA042895, R01 MH129370, and R01 MH129320 (BTS). We thank Michael Dahl for assistance, and all members of the Saunders lab for their input and support in completion of this work.

## References


1. Berke JD (2018). What does dopamine mean? Nat. Neurosci 21, 787–793. 10.1038/s41593-018-0152-y. [PubMed: 29760524]
2. Keiflin R, and Janak PH (2015). Dopamine prediction errors in reward learning and addiction: from theory to neural circuitry. Neuron 88, 247–263. 10.1016/j.neuron.2015.08.037. [PubMed: 26494275]
3. Schultz W (2006). Behavioral theories and the neurophysiology of reward. Annu. Rev. Psychol 57, 87–115. 10.1146/annurev.psych.56.091103.070229. [PubMed: 16318590]
4. Cox J, and Witten IB (2019). Striatal circuits for reward learning and decision-making. Nat. Rev. Neurosci 20, 482–494. 10.1038/s41583-019-0189-2. [PubMed: 31171839]
5. Robinson TE, and Berridge KC (1993). The neural basis of drug craving: an incentive-sensitization theory of addiction. Brain Res. Brain Res. Rev 18, 247–291. 10.1016/0165-0173(93)90013-P. [PubMed: 8401595]
6. Saunders BT, Richard JM, Margolis EB, and Janak PH (2018). Dopamine neurons create Pavlovian conditioned stimuli with circuit-defined motivational properties. Nat. Neurosci 21, 1072–1083. 10.1038/s41593-018-0191-4. [PubMed: 30038277]
7. Sharpe MJ, Chang CY, Liu MA, Batchelor HM, Mueller LE, Jones JL, Niv Y, and Schoenbaum G (2017). Dopamine transients are sufficient and necessary for acquisition of model-based associations. Nat. Neurosci 20, 735–742. 10.1038/nn.4538. [PubMed: 28368385]
8. Howe MW, and Dombeck DA (2016). Rapid signalling in distinct dopaminergic axons during locomotion and reward. Nature 535, 505–510. 10.1038/nature18942. [PubMed: 27398617]
9. Tsai H-C, Zhang F, Adamantidis A, Stuber GD, Bonci A, de Lecea L, and Deisseroth K (2009). Phasic firing in dopaminergic neurons is sufficient for behavioral conditioning. Science 324, 1080–1084. 10.1126/science.1168878. [PubMed: 19389999]
10. Keiflin R, Pribut HJ, Shah NB, and Janak PH (2019). Ventral tegmental dopamine neurons participate in reward identity predictions. Curr. Biol 29, 93–103.e3. 10.1016/j.cub.2018.11.050. [PubMed: 30581025]
11. Steinberg EE, Keiflin R, Boivin JR, Witten IB, Deisseroth K, and Janak PH (2013). A causal link between prediction errors, dopamine neurons and learning. Nat. Neurosci 16, 966–973. 10.1038/nn.3413. [PubMed: 23708143]
12. Cohen JY, Haesler S, Vong L, Lowell BB, and Uchida N (2012). Neuron-type-specific signals for reward and punishment in the ventral tegmental area. Nature 482, 85–88. 10.1038/nature10754. [PubMed: 22258508]
13. Schultz W, Dayan P, and Montague PR (1997). A neural substrate of prediction and reward. Science 275, 1593–1599. 10.1126/science.275.5306.1593. [PubMed: 9054347]
14. Breton JM, Charbit AR, Snyder BJ, Fong PTK, Dias EV, Himmels P, Lock H, and Margolis EB (2019). Relative contributions and mapping of ventral tegmental area dopamine and GABA neurons by projection target in the rat. J. Comp. Neurol 527, 916–941. 10.1002/cne.24572. [PubMed: 30393861]
15. Swanson LW (1982). The projections of the ventral tegmental area and adjacent regions: a combined fluorescent retrograde tracer and immunofluorescence study in the rat. Brain Res. Bull 9, 321–353. 10.1016/0361-9230(82)90145-9. [PubMed: 6816390]
16. Haber SN, Fudge JL, and McFarland NR (2000). Striatonigrostriatal pathways in primates form an ascending spiral from the shell to the dorsolateral striatum. J. Neurosci 20, 2369–2382. 10.1523/JNEUROSCI.20-06-02369.2000. [PubMed: 10704511]
17. Lerner TN (2020). Interfacing behavioral and neural circuit models for habit formation. J. Neurosci. Res 98, 1031–1045. 10.1002/jnr.24581. [PubMed: 31916623]
18. Belin D, and Everitt BJ (2008). Cocaine seeking habits depend upon dopamine-dependent serial connectivity linking the ventral with the dorsal striatum. Neuron 57, 432–441. 10.1016/j.neuron.2007.12.019. [PubMed: 18255035]
19. Willuhn I, Burgeno LM, Everitt BJ, and Phillips PEM (2012). Hierarchical recruitment of phasic dopamine signaling in the striatum during the progression of cocaine use. Proc Natl Acad Sci USA 109, 20703–20708. 10.1073/pnas.1213460109. [PubMed: 23184975]

20. Porrino LJ, Lyons D, Smith HR, Daunais JB, and Nader MA (2004). Cocaine self-administration produces a progressive involvement of limbic, association, and sensorimotor striatal domains. J. Neurosci 24, 3554–3562. 10.1523/JNEUROSCI.5578-03.2004. [PubMed: 15071103]
21. Yin HH, and Knowlton BJ (2006). The role of the basal ganglia in habit formation. Nat. Rev. Neurosci 7, 464–476. 10.1038/nrn1919. [PubMed: 16715055]
22. Everitt BJ, and Robbins TW (2005). Neural systems of reinforcement for drug addiction: from actions to habits to compulsion. Nat. Neurosci 8, 1481–1489. 10.1038/nn1579. [PubMed: 16251991]
23. Lüscher C, and Janak PH (2021). Consolidating the circuit model for addiction. Annu. Rev. Neurosci 44, 173–195. 10.1146/annurev-neuro-092920-123905. [PubMed: 33667115]
24. Seiler JL, Cosme CV, Sherathiya VN, Schaid MD, Bianco JM, Bridgemohan AS, and Lerner TN (2022). Dopamine signaling in the dorsomedial striatum promotes compulsive behavior. Curr. Biol 32, 1175–1188.e5. 10.1016/j.cub.2022.01.055. [PubMed: 35134327]
25. Vandaele Y, Mahajan NR, Ottenheimer DJ, Richard JM, Mysore SP, and Janak PH (2019). Distinct recruitment of dorsomedial and dorsolateral striatum erodes with extended training. eLife 8. 10.7554/eLife.49536.
26. van Elzelingen W, Warnaar P, Matos J, Bastet W, Jonkman R, Smulders D, Goedhoop J, Denys D, Arbab T, and Willuhn I (2022). Striatal dopamine signals are region specific and temporally stable across action-sequence habit formation. Curr. Biol 32, 1163–1174.e6. 10.1016/j.cub.2021.12.027. [PubMed: 35134325]
27. Coddington LT, and Dudman JT (2018). The timing of action determines reward prediction signals in identified midbrain dopamine neurons. Nat. Neurosci 21, 1563–1573. 10.1038/s41593-018-0245-7. [PubMed: 30323275]
28. Fraser KM, and Janak PH (2017). Long-lasting contribution of dopamine in the nucleus accumbens core, but not dorsal lateral striatum, to sign-tracking. Eur. J. Neurosci 46, 2047–2055. 10.1111/ejn.13642. [PubMed: 28699296]
29. Parker NF, Cameron CM, Taliaferro JP, Lee J, Choi JY, Davidson TJ, Daw ND, and Witten IB (2016). Reward and choice encoding in terminals of midbrain dopamine neurons depends on striatal target. Nat. Neurosci 19, 845–854. 10.1038/nn.4287. [PubMed: 27110917]
30. Tsutsui-Kimura I, Matsumoto H, Akiti K, Yamada MM, Uchida N, and Watabe-Uchida M (2020). Distinct temporal difference error signals in dopamine axons in three regions of the striatum in a decision-making task. eLife 9. 10.7554/eLife.62390.
31. Brown HD, McCutcheon JE, Cone JJ, Ragozzino ME, and Roitman MF (2011). Primary food reward and reward-predictive stimuli evoke different patterns of phasic dopamine signaling throughout the striatum. Eur. J. Neurosci 34, 1997–2006. 10.1111/j.1460-9568.2011.07914.x. [PubMed: 22122410]
32. Liu Y, Jean-Richard-Dit-Bressel P, Yau JO-Y, Willing A, Prasad AA, Power JM, Killcross S, Clifford CWG, and McNally GP (2020). The Mesolimbic Dopamine Activity Signatures of Relapse to Alcohol-Seeking. J. Neurosci 40, 6409–6427. 10.1523/JNEUROSCI.0724-20.2020. [PubMed: 32669355]
33. de Jong JW, Afjei SA, Pollak Dorocic I, Peck JR, Liu C, Kim CK, Tian L, Deisseroth K, and Lammel S (2019). A neural circuit mechanism for encoding aversive stimuli in the mesolimbic dopamine system. Neuron 101, 133–151.e7. 10.1016/j.neuron.2018.11.005. [PubMed: 30503173]
34. Collins AL, and Saunders BT (2020). Heterogeneity in striatal dopamine circuits: Form and function in dynamic reward seeking. J. Neurosci. Res 98, 1046–1069. 10.1002/jnr.24587. [PubMed: 32056298]
35. Mohebi A, Pettibone JR, Hamid AA, Wong J-MT, Vinson LT, Patriarchi T, Tian L, Kennedy RT, and Berke JD (2019). Dissociable dopamine dynamics for learning and motivation. Nature 570, 65–70. 10.1038/s41586-019-1235-y. [PubMed: 31118513]
36. Mohebi A, Wei W, Pelattini L, Kim K, and Berke JD (2024). Dopamine transients follow a striatal gradient of reward time horizons. Nat. Neurosci 10.1038/s41593-023-01566-3.
37. Lammel S, Lim BK, and Malenka RC (2014). Reward and aversion in a heterogeneous midbrain dopamine system. Neuropharmacology 76 Pt B, 351–359. 10.1016/j.neuropharm.2013.03.019. [PubMed: 23578393]

38. Azcorra M, Gaertner Z, Davidson C, He Q, Kim H, Nagappan S, Hayes CK, Ramakrishnan C, Fenno L, Kim YS, et al. (2023). Unique functional responses differentially map onto genetic subtypes of dopamine neurons. Nat. Neurosci 26, 1762–1774. 10.1038/s41593-023-01401-9. [PubMed: 37537242]
39. van Elzelingen W, Goedhoop J, Warnaar P, Denys D, Arbab T, and Willuhn I (2022). A unidirectional but not uniform striatal landscape of dopamine signaling for motivational stimuli. Proc Natl Acad Sci USA 119, e2117270119. 10.1073/pnas.2117270119. [PubMed: 35594399]
40. Salinas AG, Lee JO, Augustin SM, Zhang S, Patriarchi T, Tian L, Morales M, Mateo Y, and Lovinger DM (2023). Distinct sub-second dopamine signaling in dorsolateral striatum measured by a genetically-encoded fluorescent sensor. Nat. Commun 14, 5915. 10.1038/s41467-023-41581-3. [PubMed: 37739964]
41. Patriarchi T, Cho JR, Merten K, Howe MW, Marley A, Xiong W-H, Folk RW, Broussard GJ, Liang R, Jang MJ, et al. (2018). Ultrafast neuronal imaging of dopamine dynamics with designed genetically encoded sensors. Science 360. 10.1126/science.aat4422.
42. Mathis A, Mamidanna P, Cury KM, Abe T, Murthy VN, Mathis MW, and Bethge M (2018). DeepLabCut: markerless pose estimation of user-defined body parts with deep learning. Nat. Neurosci 21, 1281–1289. 10.1038/s41593-018-0209-y. [PubMed: 30127430]
43. Saunders BT, and Robinson TE (2012). The role of dopamine in the accumbens core in the expression of Pavlovian-conditioned responses. Eur. J. Neurosci 36, 2521–2532. 10.1111/j.1460-9568.2012.08217.x. [PubMed: 22780554]
44. Flagel SB, Clark JJ, Robinson TE, Mayo L, Czuj A, Willuhn I, Akers CA, Clinton SM, Phillips PEM, and Akil H (2011). A selective role for dopamine in stimulus-reward learning. Nature 469, 53–57. 10.1038/nature09588. [PubMed: 21150898]
45. Witten IB, Steinberg EE, Lee SY, Davidson TJ, Zalocusky KA, Brodsky M, Yizhar O, Cho SL, Gong S, Ramakrishnan C, et al. (2011). Recombinase-driver rat lines: tools, techniques, and optogenetic application to dopamine-mediated reinforcement. Neuron 72, 721–733. 10.1016/j.neuron.2011.10.028. [PubMed: 22153370]
46. Lee K, Claar LD, Hachisuka A, Bakhurin KI, Nguyen J, Trott JM, Gill JL, and Masmanidis SC (2020). Temporally restricted dopaminergic control of reward-conditioned movements. Nat. Neurosci 23, 209–216. 10.1038/s41593-019-0567-0. [PubMed: 31932769]
47. Flagel SB, Akil H, and Robinson TE (2009). Individual differences in the attribution of incentive salience to reward-related cues: Implications for addiction. Neuropharmacology 56 Suppl 1, 139–148. 10.1016/j.neuropharm.2008.06.027. [PubMed: 18619474]
48. Siciliano CA, and Tye KM (2019). Leveraging calcium imaging to illuminate circuit dysfunction in addiction. Alcohol 74, 47–63. 10.1016/j.alcohol.2018.05.013. [PubMed: 30470589]
49. Simpson EH, Akam T, Patriarchi T, Blanco-Pozo M, Burgeno LM, Mohebi A, Cragg SJ, and Walton ME (2024). Lights, fiber, action! A primer on in vivo fiber photometry. Neuron 112, 718–739. 10.1016/j.neuron.2023.11.016. [PubMed: 38103545]
50. Eshel N, Bukwich M, Rao V, Hemmelder V, Tian J, and Uchida N (2015). Arithmetic and local circuitry underlying dopamine prediction errors. Nature 525, 243–246. 10.1038/nature14855. [PubMed: 26322583]
51. Waelti P, Dickinson A, and Schultz W (2001). Dopamine responses comply with basic assumptions of formal learning theory. Nature 412, 43–48. 10.1038/35083500. [PubMed: 11452299]
52. Day JJ, Roitman MF, Wightman RM, and Carelli RM (2007). Associative learning mediates dynamic shifts in dopamine signaling in the nucleus accumbens. Nat. Neurosci 10, 1020–1028. 10.1038/nn1923. [PubMed: 17603481]
53. Fraser KM, Pribut HJ, Janak PH, and Keiflin R (2023). From prediction to action: dissociable roles of ventral tegmental area and substantia nigra dopamine neurons in instrumental reinforcement. J. Neurosci 10.1523/JNEUROSCI.0028-23.2023.
54. Kutlu MG, Zachry JE, Melugin PR, Tat J, Cajigas S, Isiktas AU, Patel DD, Siciliano CA, Schoenbaum G, Sharpe MJ, et al. (2022). Dopamine signaling in the nucleus accumbens core mediates latent inhibition. Nat. Neurosci 25, 1071–1081. 10.1038/s41593-022-01126-1. [PubMed: 35902648]

55. Lee RS, Mattar MG, Parker NF, Witten IB, and Daw ND (2019). Reward prediction error does not explain movement selectivity in DMS-projecting dopamine neurons. eLife 8. 10.7554/eLife.42992.
56. Moss MM, Zatka-Haas P, Harris KD, Carandini M, and Lak A (2021). Dopamine axons in dorsal striatum encode contralateral visual stimuli and choices. J. Neurosci 41, 7197–7205. 10.1523/JNEUROSCI.0490-21.2021. [PubMed: 34253628]
57. Hollon NG, Williams EW, Howard CD, Li H, Traut TI, and Jin X (2021). Nigrostriatal dopamine signals sequence-specific action-outcome prediction errors. Curr. Biol 31, 5350–5363.e5. 10.1016/j.cub.2021.09.040. [PubMed: 34637751]
58. Coddington LT, and Dudman JT (2019). Learning from Action: Reconsidering Movement Signaling in Midbrain Dopamine Neuron Activity. Neuron 104, 63–77. 10.1016/j.neuron.2019.08.036. [PubMed: 31600516]
59. Howard CD, Li H, Geddes CE, and Jin X (2017). Dynamic nigrostriatal dopamine biases action selection. Neuron 93, 1436–1450.e8. 10.1016/j.neuron.2017.02.029. [PubMed: 28285820]
60. Berridge KC (2007). The debate over dopamine's role in reward: the case for incentive salience. Psychopharmacology (Berl) 191, 391–431. 10.1007/s00213-006-0578-x. [PubMed: 17072591]
61. Wassum KM, Ostlund SB, Loewinger GC, and Maidment NT (2013). Phasic mesolimbic dopamine release tracks reward seeking during expression of Pavlovian-to-instrumental transfer. Biol. Psychiatry 73, 747–755. 10.1016/j.biopsych.2012.12.005. [PubMed: 23374641]
62. Decot HK, Namboodiri VMK, Gao W, McHenry JA, Jennings JH, Lee S-H, Kantak PA, Jill Kao Y-C, Das M, Witten IB, et al. (2017). Coordination of Brain-Wide Activity Dynamics by Dopaminergic Neurons. Neuropsychopharmacology 42, 615–627. 10.1038/npp.2016.151. [PubMed: 27515791]
63. Lohani S, Poplawsky AJ, Kim SG, and Moghaddam B (2017). Unexpected global impact of VTA dopamine neuron activation as measured by opto-fMRI. Mol. Psychiatry 22, 585–594. 10.1038/mp.2016.102. [PubMed: 27457809]
64. Al-Hasani R, Gowrishankar R, Schmitz GP, Pedersen CE, Marcus DJ, Shirley SE, Hobbs TE, Elerding AJ, Renaud SJ, Jing M, et al. (2021). Ventral tegmental area GABAergic inhibition of cholinergic interneurons in the ventral nucleus accumbens shell promotes reward reinforcement. Nat. Neurosci 24, 1414–1428. 10.1038/s41593-021-00898-2. [PubMed: 34385700]
65. Al-Hasani R, McCall JG, Shin G, Gomez AM, Schmitz GP, Bernardi JM, Pyo C-O, Park SI, Marcinkiewcz CM, Crowley NA, et al. (2015). Distinct subpopulations of nucleus accumbens dynorphin neurons drive aversion and reward. Neuron 87, 1063–1077. 10.1016/j.neuron.2015.08.019. [PubMed: 26335648]
66. Cachope R, and Cheer JF (2014). Local control of striatal dopamine release. Front. Behav. Neurosci 8, 188. 10.3389/fnbeh.2014.00188. [PubMed: 24904339]
67. Yang H, de Jong JW, Tak Y, Peck J, Bateup HS, and Lammel S (2018). Nucleus accumbens subnuclei regulate motivated behavior via direct inhibition and disinhibition of VTA dopamine subpopulations. Neuron 97, 434–449.e4. 10.1016/j.neuron.2017.12.022. [PubMed: 29307710]
68. de Jong JW, Liang Y, Verharen JPH, Fraser KM, and Lammel S (2024). State and rate-of-change encoding in parallel mesoaccumbal dopamine pathways. Nat. Neurosci 27, 309–318. 10.1038/s41593-023-01547-6. [PubMed: 38212586]
69. Di Chiara G (2002). Nucleus accumbens shell and core dopamine: differential role in behavior and addiction. Behav. Brain Res 137, 75–114. 10.1016/s0166-4328(02)00286-3. [PubMed: 12445717]
70. Beyene M, Carelli RM, and Wightman RM (2010). Cue-evoked dopamine release in the nucleus accumbens shell tracks reinforcer magnitude during intracranial self-stimulation. Neuroscience 169, 1682–1688. 10.1016/j.neuroscience.2010.06.047. [PubMed: 20600644]
71. Sackett DA, Saddoris MP, and Carelli RM (2017). Nucleus accumbens shell dopamine preferentially tracks information related to outcome value of reward. eNeuro 4. 10.1523/ENEURO.0058-17.2017.
72. Saddoris MP, Cacciapaglia F, Wightman RM, and Carelli RM (2015). Differential dopamine release dynamics in the nucleus accumbens core and shell reveal complementary signals for error prediction and incentive motivation. J. Neurosci 35, 11572–11582. 10.1523/JNEUROSCI.2344-15.2015. [PubMed: 26290234]

73. Zahm DS, and Brog JS (1992). On the significance of subterritories in the “accumbens” part of the rat ventral striatum. Neuroscience 50, 751–767. 10.1016/0306-4522(92)90202-d. [PubMed: 1448200]
74. Swanson LW (2005). Anatomy of the soul as reflected in the cerebral hemispheres: neural circuits underlying voluntary control of basic motivated behaviors. J. Comp. Neurol 493, 122–131. 10.1002/cne.20733. [PubMed: 16254987]
75. Wise RA (2009). Roles for nigrostriatal--not just mesocorticolimbic--dopamine in reward and addiction. Trends Neurosci. 32, 517–524. 10.1016/j.tins.2009.06.004. [PubMed: 19758714]
76. Ilango A, Kesner AJ, Keller KL, Stuber GD, Bonci A, and Ikemoto S (2014). Similar roles of substantia nigra and ventral tegmental dopamine neurons in reward and aversion. J. Neurosci 34, 817–822. 10.1523/JNEUROSCI.1703-13.2014. [PubMed: 24431440]
77. Markowitz JE, Gillis WF, Jay M, Wood J, Harris RW, Cieszkowski R, Scott R, Brann D, Koveal D, Kula T, et al. (2023). Spontaneous behaviour is structured by reinforcement without explicit reward. Nature 614, 108–117. 10.1038/s41586-022-05611-2. [PubMed: 36653449]
78. Hamilos AE, Spedicato G, Hong Y, Sun F, Li Y, and Assad JA (2021). Slowly evolving dopaminergic activity modulates the moment-to-moment probability of reward-related self-timed movements. eLife 10. 10.7554/eLife.62583.
79. Dodson PD, Dreyer JK, Jennings KA, Syed ECJ, Wade-Martins R, Cragg SJ, Bolam JP, and Magill PJ (2016). Representation of spontaneous movement by dopaminergic neurons is cell-type selective and disrupted in parkinsonism. Proc Natl Acad Sci USA 113, E2180–8. 10.1073/pnas.1515941113. [PubMed: 27001837]
80. da Silva JA, Tecuapetla F, Paixão V, and Costa RM (2018). Dopamine neuron activity before action initiation gates and invigorates future movements. Nature 554, 244–248. 10.1038/nature25457. [PubMed: 29420469]
81. Matityahu L, Gilin N, Sarpong GA, Atamna Y, Tiroshi L, Tritsch NX, Wickens JR, and Goldberg JA (2023). Acetylcholine waves and dopamine release in the striatum. Nat. Commun 14, 6852. 10.1038/s41467-023-42311-5. [PubMed: 37891198]
82. Krok AC, Maltese M, Mistry P, Miao X, Li Y, and Tritsch NX (2023). Intrinsic dopamine and acetylcholine dynamics in the striatum of mice. Nature 621, 543–549. 10.1038/s41586-023-05995-9. [PubMed: 37558873]
83. Howe M, Ridouh I, Allegra Mascaro AL, Larios A, Azcorra M, and Dombeck DA (2019). Coordination of rapid cholinergic and dopaminergic signaling in striatum during spontaneous movement. eLife 8. 10.7554/eLife.44903.
84. Ambrosi P, and Lerner TN (2022). Striatonigrostriatal circuit architecture for disinhibition of dopamine signaling. Cell Rep. 40, 111228. 10.1016/j.celrep.2022.111228. [PubMed: 35977498]
85. Lerner TN, Shilyansky C, Davidson TJ, Evans KE, Beier KT, Zalocusky KA, Crow AK, Malenka RC, Luo L, Tomer R, et al. (2015). Intact-Brain Analyses Reveal Distinct Information Carried by SNc Dopamine Subcircuits. Cell 162, 635–647. 10.1016/j.cell.2015.07.014. [PubMed: 26232229]
86. Lee J, Wang W, and Sabatini BL (2020). Anatomically segregated basal ganglia pathways allow parallel behavioral modulation. Nature Neuroscience.
87. Willuhn I, Burgeno LM, Groblewski PA, and Phillips PEM (2014). Excessive cocaine use results from decreased phasic dopamine signaling in the striatum. Nat. Neurosci 17, 704–709. 10.1038/nn.3694. [PubMed: 24705184]
88. Clark JJ, Collins AL, Sanford CA, and Phillips PEM (2013). Dopamine encoding of Pavlovian incentive stimuli diminishes with extended training. J. Neurosci 33, 3526–3532. 10.1523/JNEUROSCI.5119-12.2013. [PubMed: 23426680]
89. Pascoli V, Hiver A, Van Zessen R, Loureiro M, Achargui R, Harada M, Flakowski J, and Lüscher C (2018). Stochastic synaptic plasticity underlying compulsion in a model of addiction. Nature 564, 366–371. 10.1038/s41586-018-0789-4. [PubMed: 30568192]
90. Pascoli V, Terrier J, Hiver A, and Lüscher C (2015). Sufficiency of mesolimbic dopamine neuron stimulation for the progression to addiction. Neuron 88, 1054–1066. 10.1016/j.neuron.2015.10.017. [PubMed: 26586182]

91. Rothwell PE, Hayton SJ, Sun GL, Fuccillo MV, Lim BK, and Malenka RC (2015). Input- and Output-Specific Regulation of Serial Order Performance by Corticostriatal Circuits. Neuron 88, 345–356. 10.1016/j.neuron.2015.09.035. [PubMed: 26494279]
92. Poldrack RA, Sabb FW, Foerde K, Tom SM, Asarnow RF, Bookheimer SY, and Knowlton BJ (2005). The neural correlates of motor skill automaticity. J. Neurosci 25, 5356–5364. 10.1523/JNEUROSCI.3880-04.2005. [PubMed: 15930384]
93. Lee J, and Sabatini BL (2020). Striatal indirect pathway mediates action switching via modulation of collicular dynamics. BioRxiv. 10.1101/2020.10.01.319574.
94. Aoki S, Smith JB, Li H, Yan X, Igarashi M, Coulon P, Wickens JR, Ruigrok TJ, and Jin X (2019). An open cortico-basal ganglia loop allows limbic control over motor output via the nigrothalamic pathway. eLife 8. 10.7554/eLife.49995.
95. Hamid AA, Frank MJ, and Moore CI (2021). Wave-like dopamine dynamics as a mechanism for spatiotemporal credit assignment. Cell 184, 2733–2749.e16. 10.1016/j.cell.2021.03.046. [PubMed: 33861952]
96. Rehani R, Atamna Y, Tiroshi L, Chiu W-H, de Jesús Aceves Buendía J, Martins GJ, Jacobson GA, and Goldberg JA (2019). Activity patterns in the neuropil of striatal cholinergic interneurons in freely moving mice represent their collective spiking dynamics. eNeuro 6. 10.1523/ENEURO.0351-18.2018.
97. Nath T, Mathis A, Chen AC, Patel A, Bethge M, and Mathis MW (2019). Using DeepLabCut for 3D markerless pose estimation across species and behaviors. Nat. Protoc 14, 2152–2176. 10.1038/s41596-019-0176-0. [PubMed: 31227823]
98. Insafutdinov E, Pishchulin L, Andres B, Andriluka M, and Schiele B (2016). DeeperCut: A Deeper, Stronger, and Faster Multi-person Pose Estimation Model. In Computer vision – ECCV 2016 Lecture notes in computer science., Leibe B, Matas J, Sebe N, and Welling M, eds. (Springer International Publishing), pp. 34–50. 10.1007/978-3-319-46466-4_3.

## Highlights

- VTA DA drives learning and spatiotemporally heterogeneous DA signals in striatum
- Cue-evoked DA emerges in the NAc core and DMS, but not shell or DLS
- NAc core and DMS DA reflect movement invigoration and prediction errors
- SNc DA drives learning but does not engage prediction-related striatal DA encoding

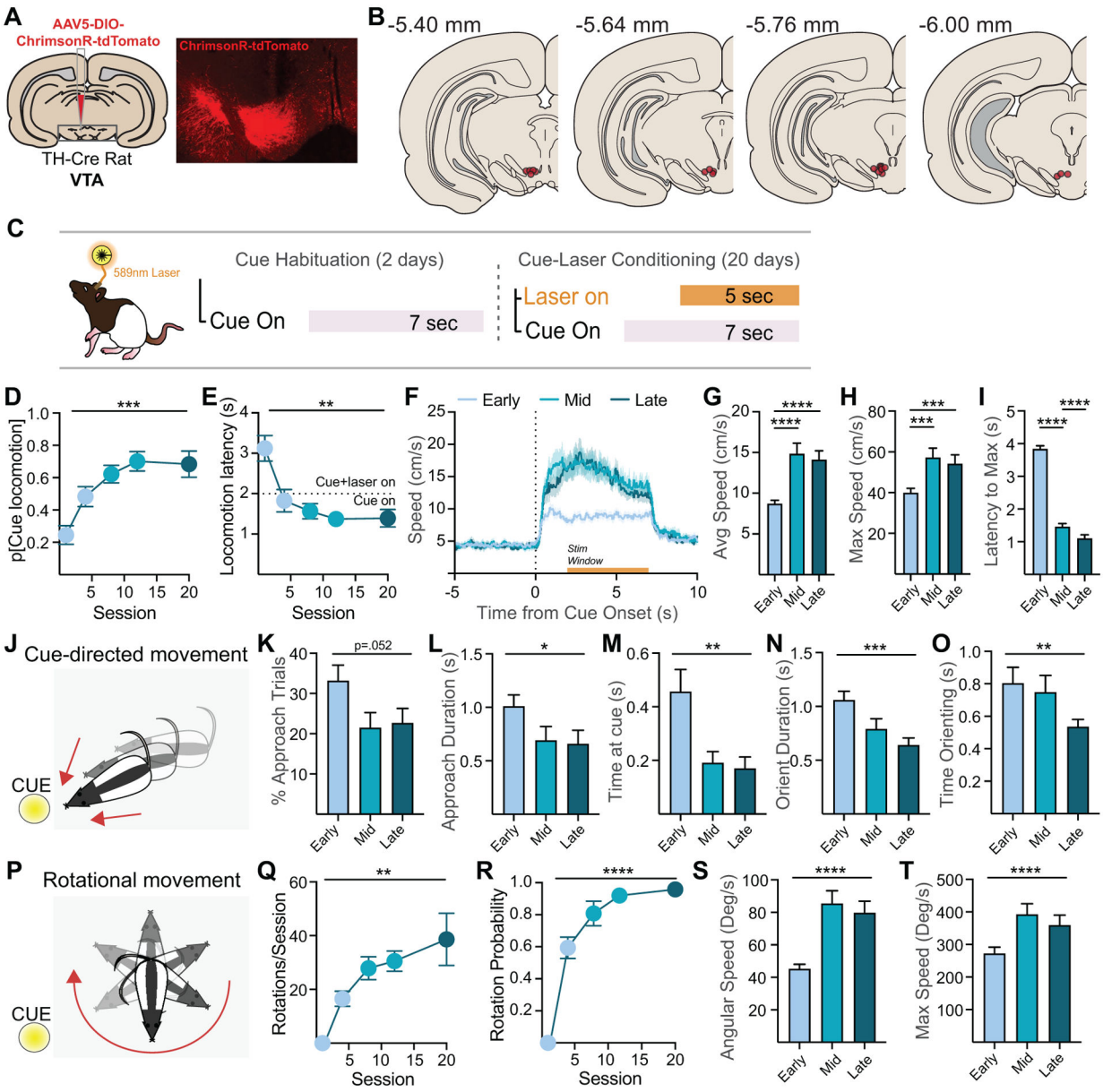


**Figure 1. VTA dopamine neurons drive cue learning and vigorous behavior.**

A) ChrimsonR-tdTomato was expressed in dopamine neurons in TH-cre rats (N=20) and B) optic fibers were inserted over the VTA. C) Optogenetic Pavlovian conditioning. D) Across training, conditioned responses (movement) emerged with high probability. E) The latency of locomotion onset decreased across sessions. F) Movement was tightly locked to cue onset, increasing in speed across the early (days 1–2), middle (days 10–12), and late (days 19–20) phases of training. Both average G) and maximum H) speed increased between early and middle/late training phases. I) Latency to reach maximum speed decreased across each training phase. J) Conditioned behavioral responses were directed at the cue. K) Classification using DLC showed a trending decrease in trials containing an approach response across training. L) Approach duration and M) the time spent at the cue across trials decreased across training. N) The length of cue orientations decreased and O)

the amount of orientation decreased as training progressed. P) As training progressed, cue-evoked movement evolved into a vigorous, rotational pattern. Rotation did not occur early in training but increased robustly in Q) number and R) probability across training. Correspondingly, S) the average and T) maximum angular speed during cue presentations increased across training. See also Figure S1. ****p<.0001, ***p<.001, **p<.01, *p<.05.

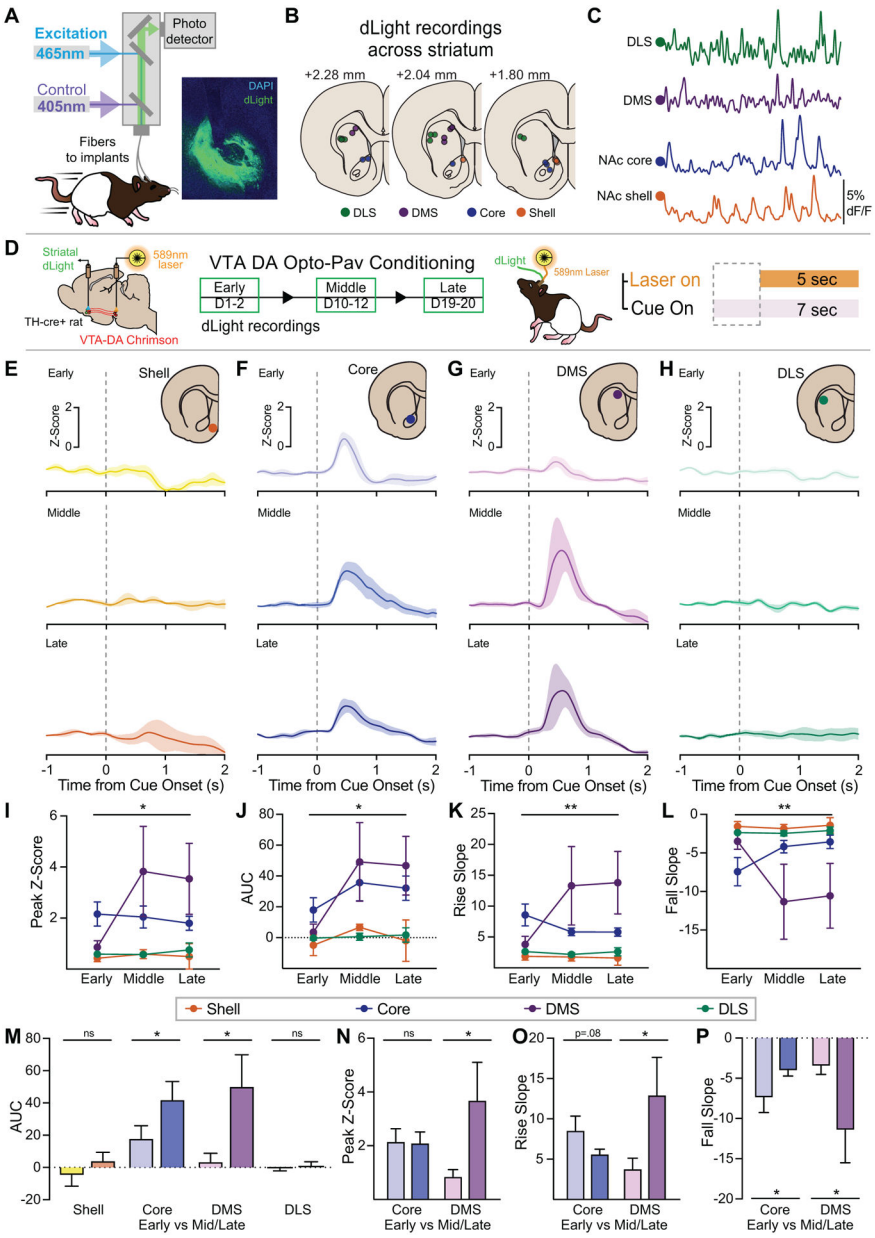


**Figure 2. Spatiotemporally heterogeneous conditioned dopamine signals develop to VTA dopamine neuron predictive cues.**

A) Fiber photometry system and analysis. The dopamine biosensor dLight 1.3b was expressed in the striatum of TH-cre rats expressing ChrimsonR in VTA dopamine neurons. B) Recording locations in four striatal regions: the NAc medial shell (n=4), NAc core (n=6), DMS (n=6), and DLS (n=9). C) Robust spontaneous dopamine fluctuations were identified in each region. D) dLight signals were recorded across optogenetic Pavlovian conditioning in three training phases: early (days 1–2), middle (days 10–12), and late (days 19–20). E) In the medial NAc shell, cue-evoked dopamine signals did not emerge at any training phase. F) In the NAc core, a phasic dopamine response emerged, which remained stable. G) In the DMS, cue-evoked signals emerged at the middle/late phases. H) In the DLS, cue-evoked signals did not emerge. I-L) Cue onset-related signal dynamics, including signal peak, AUC,

and the rise and fall slopes of peak signal, varied across region and training phase. M) AUC of cue-evoked signal increased only in the core and DMS regions. N) The peak Z-score increased in the DMS but not core. O) The rise slope of the cue-evoked signal increased in the DMS only. P) The fall slope of the peak signal decreased in the core and increased in the DMS. See also Figures S3, S4, S6. **p<.01, *p<.05.

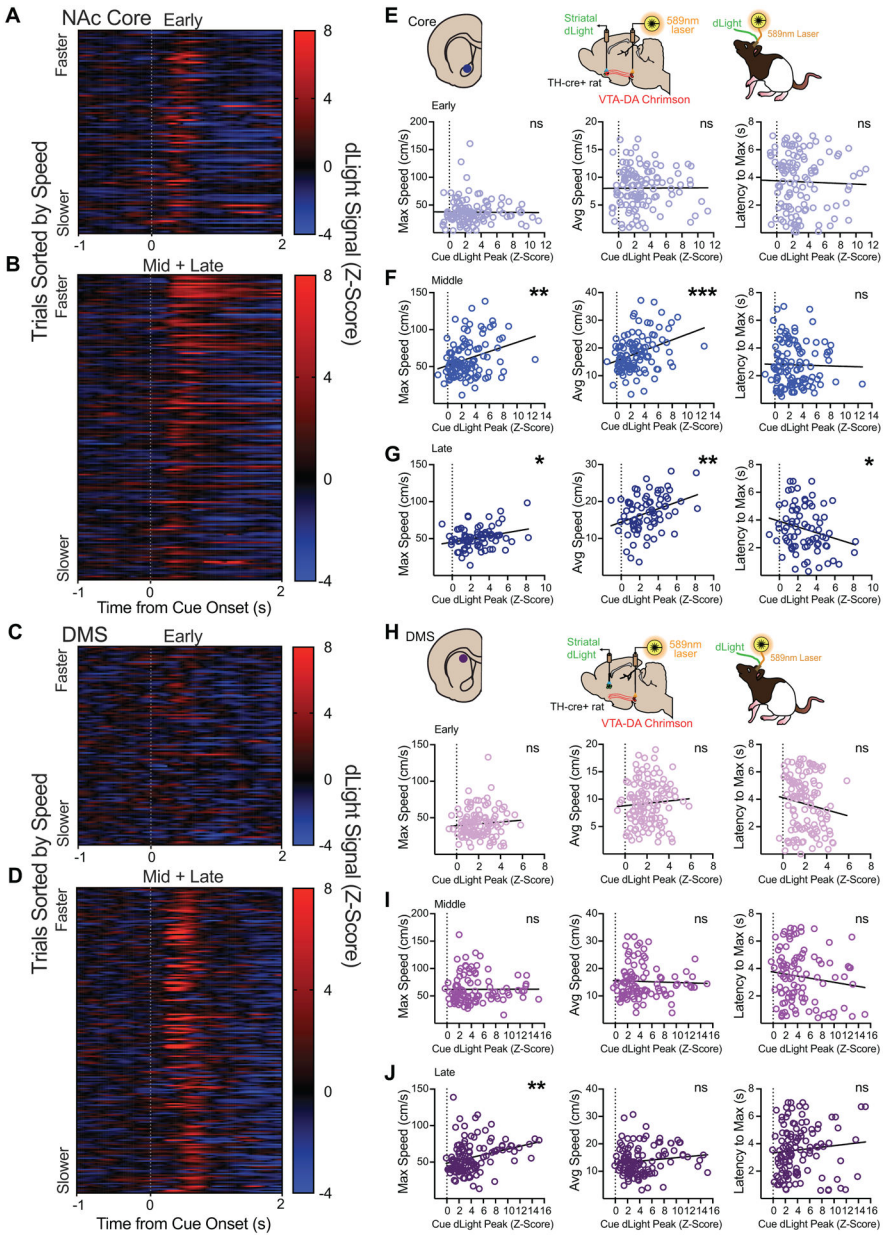


**Figure 3. VTA cue-evoked dopamine signals in the NAc core predict conditioned movement vigor.**

A) Heatmap of Z-scored NAc core dLight signals for the early versus B) mid/late training phases. Each row is a trial sorted as a function of the average speed. Heatmaps for C) early and D) mid/late DMS cue signals. E-G) Pearson correlations between the peak cue-evoked signal in the NAc core and maximum speed, average speed, and latency to maximum speed, trial by trial, for each training phase. Cue-evoked dLight in the core was not correlated with any speed measure E) early, but positive correlations with maximum and average speed emerged in the F) middle and G) late phases, while a negative correlation with latency to maximum speed emerged in the late phase. H-J) Corresponding cue signal versus speed variable correlations for the DMS. Across these analyses, cue-evoked dLight in the DMS

was only correlated with the maximum speed in the J) late phase. See also Figures S2, S3. ***p<.001, **p<.01, *p<.05.

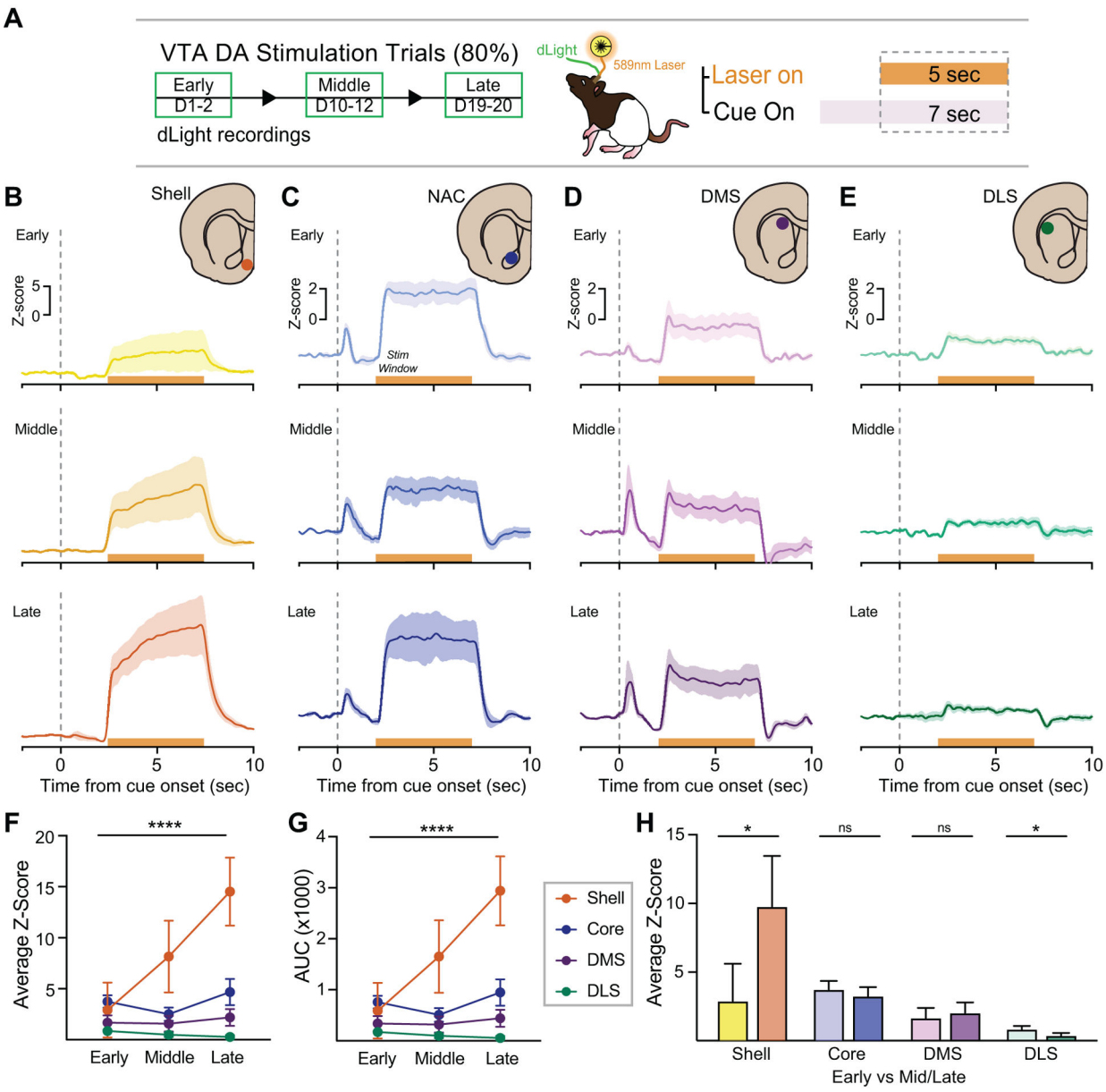


**Figure 4. VTA dopamine neurons drive dopamine signaling preferentially in the medial striatum.**

A). During optogenetic conditioning recording sessions, cues were paired with optogenetic stimulation of VTA dopamine neurons on 80% (20/25) of trials. B-C) Optogenetic activation of VTA dopamine neurons (20Hz, 5sec) produced different patterns of dopamine signaling across striatal targets. B) Large laser-evoked dopamine signals were present from training onset in the NAc medial shell, and increased in magnitude across training. C) Robust laser evoked dopamine signals were present in the NAc core, and D) DMS. E) In contrast, optogenetic stimulation of VTA dopamine neurons evoked minimal dopamine signals in the DLS. F,G,H) Stimulation-evoked dLight signals increased in the shell, remained stable in the core and DMS, and decreased in the DLS, across training. See also Figures S2, S4. ****p<.0001, *p<.05.

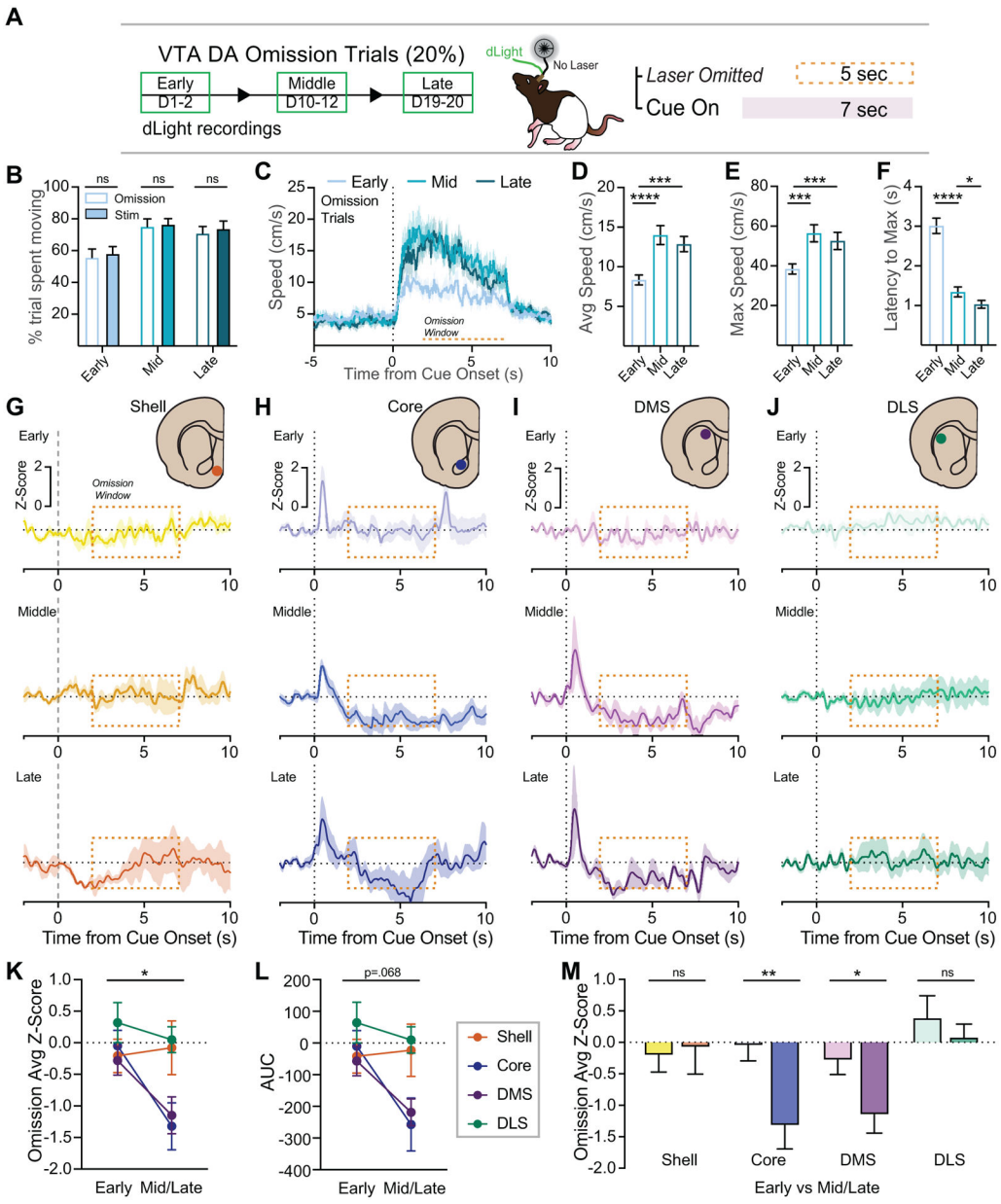


**Figure 5. Dopamine signals in the NAc core and DMS, but not shell or DLS, report VTA dopamine prediction errors.**

A) On dLight recording sessions, laser delivery was omitted on 20% of cue presentations. B) Rats spent similar amounts of time moving during cue presentations on stimulation and omission trials. C) On omission trials, movement was tightly locked to cue onset and offset, increasing in D) average speed E) and maximum speed, and F) decreasing latency to reach maximum speed across training. G) Dopamine signals in the NAc medial shell did not systematically change during the laser omission window. H) In the NAc core and I) DMS, a laser omission-related reduction in dopamine signals emerged across the middle and late training phases. J) Laser omission-related changes in dopamine signal did not emerge in the DLS at any stage. K,L) During the omission window the average signal z-score varied across region and training phase, with a trend for AUC. M) The average Z-score of

omission-related signals decreased in the core and the DMS, but not in the shell or DLS, across training. See also Figure S6. ****p<.0001, ***p<.001, **p<.01, *p<.05.

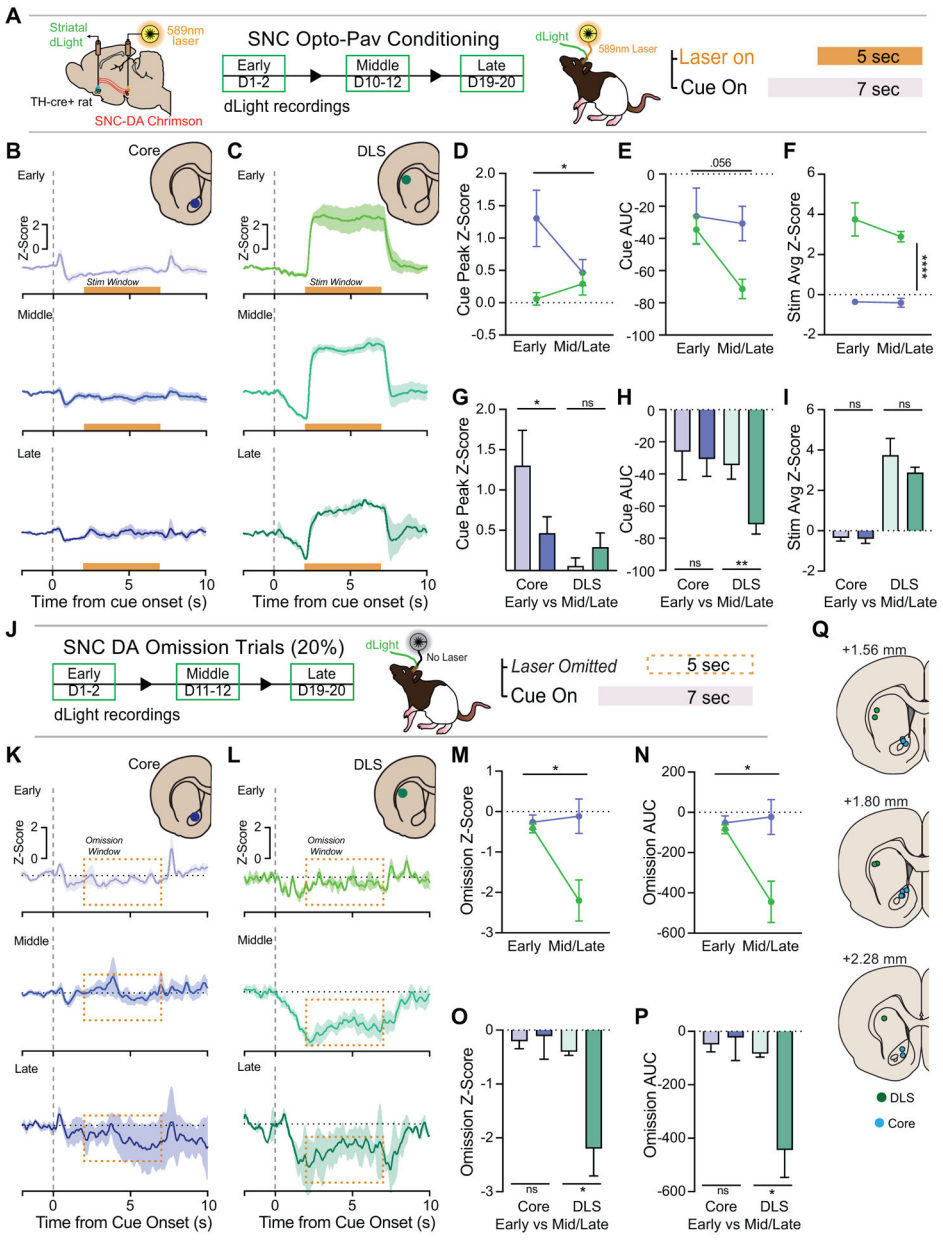


**Figure 6. Heterogeneous striatal dopamine signals emerge during learning driven by SNC dopamine neuron stimulation.**

A) Chrimson was targeted to SNC dopamine neurons and dLight signals were recorded in the NAc core (n=9) and DLS (n=5) across optogenetic Pavlovian conditioning. B) In the core, there was an initial cue response, which diminished with training. C) In the DLS, no positive peak occurred, but a steady negative ramp emerged to the cue. D,E,G,H) Quantification of the cue peak and AUC measures showed that the positive core peak diminished with training, and the cue AUC for the DLS became more negative. F,I) Strong laser-evoked dLight was seen in the DLS across training, but not in the core at any stage. J) On dLight recording sessions, laser delivery was omitted on 20% of cue presentations. K) Core signals did not systematically change during omission. L) In the DLS, dopamine ramped down at cue onset as training progressed. Quantification of the M,O) z-score and

N,P) AUC during the omission period confirmed that core signals did not change, but DLS signals became more negative. Q) Recording fiber placements in the DLS and core. See also Figures S5, S6. ****p<.0001, **p<.01, *p<.05.

## Key resources table

| REAGENT or RESOURCE | SOURCE | IDENTIFIER |
|---|---|---|
| Antibodies | | |
| N/A | | |
| Bacterial and virus strains | | |
| AAV5-hSyn-FLEX-ChrimsonR-tdTomato | Edward Boyden | Addgene 84483 |
| AAV5-hSyn-dLight1.3b | Lin Tian | Addgene 125560 |
| Biological samples | | |
| N/A | | |
| Chemicals, peptides, and recombinant proteins | | |
| Carprofen injectable solution | Santa Cruz Biotechnology, Inc. | sc-395914Rx |
| Vectashield mounting medium | VectorLabs | H-1000-10 |
| Jet liquid clear | Lang Dental | NA |
| Jet denture repair powder | Lang Dental | NA |
| Critical commercial assays | | |
| Experimental models: Cell lines | | |
| N/A | | |
| Experimental models: Organisms/strains | | |
| Long Evans TH-cre rats [Tg(TH-Cre)3.1Deis] | RRRC | https://www.rrrc.us/Strain/?x=659 |
| Oligonucleotides | | |
| N/A | | |
| Recombinant DNA | | |
| N/A | | |
| Software and algorithms | | |
| MATLAB | Mathworks | RRID:SCR_001622 |
| Synapse software | Tucker-Davis Technologies | https://www.tdt.com/component/synapse-software/ |
| Fiber photometry analysis code | Tucker-Davis Technologies | https://www.tdt.com/docs/fiber-photometry-user-guide/data-analysis/ |
| DeepLabCut behavioral analysis code | Alexander Mathis, Mackenzie Mathis, Tanmay Nath, Jessy Lauer | https://pypi.org/project/deeplabcut/ |
| Other | | |
| Fiberoptic cannula for optogenetics | RWD Life Science Inc. | R-FOC-BF300C39NA |
| Fiberoptic cannula for fiber photometry | Doric Lenses | MFC_300/330-0.37_9mm_MF2.5_FLT |
| Mono fiberoptic patchcords | Doric Lenses | MFP_400/460/900-0.48_1m_FCM-MF1.25 |
| Fiber photometry workstations | Tucker-Davis Technologies | RZ5P |
| Newport photoreceivers | Doric Lenses | NPM_2151_FOA_FC |
| Fluorescence Minicubes | Doric Lenses | FMC4_AE(405)_E(460–490)_F(500–550)_S |
| LED driver | Doric Lenses | LEDD_4 ×1 |
| Connectorized LD: 405 nm | Doric Lenses | CLED_405 |
| Connectorized LD: 465 nm | Doric Lenses | CLED_465 |

| REAGENT or RESOURCE | SOURCE | IDENTIFIER |
|---|---|---|
| Epifluorescence microscope | Keyence | BZ-X |
| Dual small animal stereotaxic instrument | David Kopf Instrumental | Model 942 |
| Cryostat | Leica Biosystems | CM1900 |